Jitter in piecewise-smooth dynamical systems with intersecting discontinuity surfaces

M.R. Jeffrey[†], G. Kafanas[†], and D.J.W. Simpson[‡]

[†]*Department of Engineering Mathematics, University of Bristol, Bristol, UK*

[‡]*Institute of Fundamental Sciences, Massey University, Palmerston North, New Zealand*

(Dated: April 11, 2018)

Differential equations that switch between different modes of behaviour across a surface of discontinuity are used to model, for example, electronic switches, mechanical contact, predator-prey preference changes, and genetic or cellular regulation. Switching in such systems is unlikely to occur precisely at the ideal discontinuity surface, but instead can involve various spatio-temporal delays or noise. If a system switches between more than two modes, across a boundary formed by the intersection of discontinuity surfaces, then its motion along that intersection becomes highly sensitive to such non-idealities. If switching across the surfaces is affected by hysteresis, time delay, or discretization, then motion along the intersection can be affected by erratic variation that we characterize as 'jitter'. Introducing noise, or smoothing out the discontinuity, instead leads to steady motion along the intersection well described by the so-called *canopy* extension of Filippov's sliding concept (which applies when the discontinuity surface is a simple hypersurface). We illustrate the results with numerical experiments and an example from power electronics, providing explanations for the phenomenon as far as they are known.

1. INTRODUCTION

Discontinuities are increasingly used to model abrupt features of dynamic systems, from the position of electrical switches [1], the mode of contact between physical objects [2, 3], resistivity of superconductors across the critical temperature [4], reflectivity of surfaces such as across ice-lines in climate models [5], or changes in predatory, social, or regulatory behaviours of living organisms [6–8]. In many such systems it is possible for the dynamics to evolve along the locus of discontinuity, a phenomenon called *sliding*. Given the ever more general contexts in which discontinuities arise, a particular question of interest is how robust sliding motion is to perturbations. In applications, switching between values across a discontinuity may involve time delays, hysteresis, and noise, all features whose effects are difficult to derive both analytically and numerically.

This paper revisits results from [9] that have taken on new significance recently in the light of growing interest from both applications and fundamental theory. In studying motion along the

boundary of several open regions $\mathcal{Q}_1$, $\mathcal{Q}_2$, ..., given that evolution inside those regions is given by

$$\dot{\mathbf{x}} = \{\mathbf{f}_i(\mathbf{x}) \text{ if } \mathbf{x} \in \mathcal{Q}_i \ , \ i = 1, 2, \dots \} \ , \tag{1}$$

Alexander and Seidman discussed in [9, 10] two alternative ways of deriving the solutions $\mathbf{x}(t)$. While in [10] they predicted steady determinable motion, in [9] they uncovered an instability that causes sliding motion to vary erratically, a phenomenon we call here *jitter*.

Jitter is distinct from another phenomenon associated with discontinuities called *chatter*. A system may chatter back and forth across a boundary as it is kicked by a pair of vector fields that point towards the boundary from either side. Typically this averages out in the long term into steady motion along the boundary. Jitter is instead a series of sharp changes in that long term motion, induced by small scale perturbations (of which chatter is an example).

The outcome of the Alexander-Seidman work was a conflicting pair of predictions for how solutions $\mathbf{x}(t)$ evolve along a set on the boundary of the regions $\mathcal{Q}_1$, $\mathcal{Q}_2$, ... Steady determinable motion along the intersection is predicted if the equations are 'blended' (or interpolated) across the boundaries between regions $\mathcal{Q}_i$. Jittery motion is instead predicted if solutions $\mathbf{x}(t)$ slightly overshoot the boundaries before switching to the field $\mathbf{f}_i$ appropriate in each region $\mathcal{Q}_i$. It is assumed that the $\mathbf{f}_i$ are unrelated vector fields that point towards the boundary, and that the boundary consists of transversally intersecting smooth hypersurfaces, such that, local to their intersection, q hypersurfaces (e.g. coordinate planes $x = 0$, $y = 0$, ...) divide space into 2^q regions $\mathcal{Q}_1$, ..., $\mathcal{Q}_{2^q}$, as shown in fig. 1 for $q = 2$.

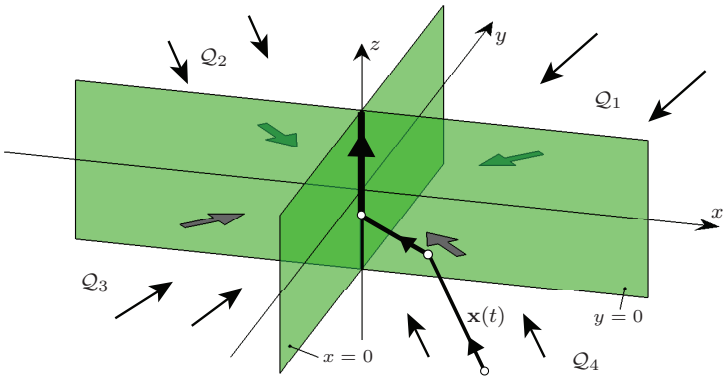

FIG. 1: A vector field that is discontinuous across the surfaces $x = 0$ and $y = 0$, and smooth in $\mathcal{Q}_1$, $\mathcal{Q}_2$, $\mathcal{Q}_3$, $\mathcal{Q}_4$,. Sliding motion is possible along the discontinuity surfaces. A trajectory is shown flowing from $\mathcal{Q}_4$, to the surface $y = 0$, to the intersection $x = y = 0$; our interest is in the latter portion of this motion.

The problem of interest is then simply to determine the speed of motion along $x = y = 0$ in fig. 1, for a system in coordinates $\mathbf{x} = (x, y, z)$ where space is divided into quadrants $\mathcal{Q}_1$, $\mathcal{Q}_2$, $\mathcal{Q}_3$, $\mathcal{Q}_4$, by the coordinate planes $x = 0$ and $y = 0$. The unshaded region in fig. 2 indicates the set (or 'hull') of all possible speeds of motion if $\mathbf{x}(t)$ evolves in increments along each field $\mathbf{f}_i$, e.g. $\Delta\mathbf{x} = \mathbf{f}_i \Delta t$. The simplest analytical approach is to blend the vector fields across the discontinuity surfaces, which results in steady motion along $x = y = 0$ (dashed curve). In fact the speed along $x = y = 0$ depends on the fine details of how the system switches between the fields $\mathbf{f}_i$. If that switching involves hysteresis, for example, the result is more erratic motion (full curve); the abrupt kinks in this curve are what we call jitter.

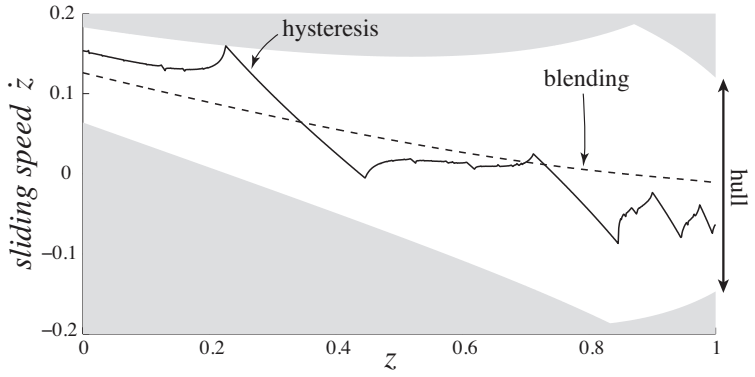

FIG. 2: Speed of sliding $\dot{z}$ along the intersection of the discontinuity surfaces $x = 0$ and $y = 0$ at different values of z, for an example of the piecewise-smooth system (1) (example follows in section 2), showing the two Alexander-Seidman alternatives with hysteresis (full curve) or blending (dashed curve), and the set of all possible sliding speeds (unshaded region).

The particulars of this example and the simulation methods will be given in section 2, including how they fit into Filippov's theory of differential inclusions, and adding generalizations of the phenomenon if switching involves other sources of spatial or temporal delays or stochasticity. The latter point the way to a generalization of the phenomenon of jitter with wide-reaching practical significance. We outline the conditions that make jitter possible in section 3. A rigorous explanation for the phenomenon is only known in the case when it is induced by hysteresis, connected to nonsmooth circle maps, which we describe in section 4. A testable physical application from electronics is described in section 5, and we make some concluding remarks in section 6.

To those who have dealt with discontinuous or 'stiff' systems, either numerically or experimentally, it might not be surprising that simulating a set of equations across a discontinuity results in some irregular or unpredictable behaviour. Jitter, however, reveals a particularly erratic and yet

structured pattern to such unpredictability. A brief explanation is that when a non-ideal system evolves approximately along a discontinuity surface, the dynamics finds an attractor that approximates, in some ε-neighbourhood, ideal sliding exactly along the surface. The same is true a an intersection of discontinuity surfaces, but the attractor can be sensitive to parameters of the vector field or the switching method, undergoing numerous bifurcations that affect the speed of sliding motion ($\dot{z}$ in fig. 2), manifesting as jitter (the abrupt change in gradient along the hysteresis graph in fig. 2).

The problem of motion along the intersection of discontinuity surfaces was left open in Filippov's influential work [11], and has recently been taken up from a variety of perspectives based on practical considerations of how to model dynamics around discontinuities, see e.g. [9, 10, 12–16], or on more theoretical considerations such as equivalence classes and stability, see e.g. [17, 18] and references therein. The Alexander-Seidman result, and its extensions discussed here, reveal much greater intricacy in the applied problem than anticipated elsewhere in the literature.

2. JITTER: NUMERICAL EXPERIMENTS

We begin with a sample of numerical simulations illustrating the phenomenon of jitter.

Consider a set of ordinary differential equations

$$\dot{\mathbf{x}} = \mathbf{f}(\mathbf{x}) = \{\mathbf{f}_i(\mathbf{x}) \quad \text{for } \mathbf{x} \in \mathcal{Q}_i \ , \quad i = 1, \ldots, m\} \ , \tag{2}$$

which is smooth except on a set of hypersurfaces Σ that partition the space of $\mathbf{x}$ into regions $\mathcal{Q}_1, \ldots, \mathcal{Q}_m$. Let $\mathbf{f}_1, \ldots \mathbf{f}_m$ be independent smooth vector fields, each of which is smooth in a neighbourhood of the closure of $\mathcal{Q}_i$ (which ensures that our implementations of switching, introduced later, are well-defined).

To simulate solutions of (2) we take an initial condition in one of the quadrants $\mathcal{Q}_i$ in mode $M = i$, then follow the algorithm:

(A.i) Solve the system $\dot{\mathbf{x}} = \mathbf{f}_i(\mathbf{x})$ in mode $M = i$ and evolve forward in time.

(A.ii) Detect when a condition $\mathrm{Imp}(\mathbf{x}, M)$ is satisfied, and update the mode $M = i$ to $M = i'$.

(A.iii) Repeated steps (i)-(ii), updating the mode M each time.

The condition $\mathrm{Imp}(\mathbf{x}, M)$ ideally represents a switch between modes as the state $\mathbf{x}(t)$ crosses a discontinuity surface between regions $\mathcal{Q}_i$ and $\mathcal{Q}_{i'}$, but its precise conditions define an *implementation* of the switch. This may involve spatial or temporal delays or stochasticity, in detecting the

discontinuity surface or in enacting the switch. A number of implementation conditions $\mathrm{Imp}(\mathbf{x}, M)$ will be considered in section 2 B-2 F.

Following this algorithm we then carry out simulations to find the speed of sliding along a discontinuity surface between regions $\mathcal{Q}_1$, $\mathcal{Q}_2$, ..., as follows.

Let $\mathbf{x}(t)$ evolve along an ε-infinitesimal neighbourhood of the discontinuity surfaces for a time interval $[0, T]$, switching between modes $M = 1, 2, \ldots, m$, at a sequence of times $t_1, t_2, \ldots, t_r$, where $0 = t_0 < t_1 < t_2 < \cdots < t_r = T$. Thus $\mathbf{x}(t)$ evolves along a different vector field $\mathbf{f}_i$ in mode $M = i$ on each time interval (t_{j-1}, t_j) for some $i = \{1, \ldots, m\}$ and $j \in \{1, \ldots, r\}$. Let γ_i denote the total proportion of the time T spent in mode i,

$$\gamma_i = \frac{1}{T} \sum_{j=1}^{r} \begin{cases} t_j - t_{j-1} & \text{if } M = i, \\ 0 & \text{if } M \neq i\,, \end{cases} \tag{3}$$

then the total change in $\mathbf{x}(t)$ over the time increment T is

$$\frac{\Delta \mathbf{x}}{T} = \left\{ \sum_{i=1} \gamma_i \mathbf{f}_i(\mathbf{x}) \quad : \quad \gamma_i \geq 0, \ \sum_{i=1}^{m} \gamma_i = 1 \right\}. \tag{4}$$

We will use this to find the coefficients γ_i from simulations. We describe (4) as the effective vector field followed by the trajectory of $\mathbf{x}(t)$, since in the limit $T \to 0$ this gives an effective equation of motion,

$$\dot{\mathbf{x}} = \mathbf{f}_{\text{eff}}(\mathbf{x}) = \left\{ \sum_{i=1} \gamma_i \mathbf{f}_i(\mathbf{x}) \quad : \quad \gamma_i \geq 0, \ \sum_{i=1}^{m} \gamma_i = 1 \right\}. \tag{5}$$

If $\mathbf{x}$ lies inside a region $\mathcal{Q}_i$ far from any discontinuity surface, then $\gamma_i = 1$ and $\gamma_j = 0$ for all other $i \neq j$, hence $\mathbf{f}_{\text{eff}}(\mathbf{x}) = \mathbf{f}_i(\mathbf{x})$. If $\mathbf{x}$ lies on the boundary between just two modes, say $\mathcal{Q}_1$ and $\mathcal{Q}_2$, then (5) simplifies to $\mathbf{f}_{\text{eff}}(\mathbf{x}) = \gamma_1 \mathbf{f}_1(\mathbf{x}) + (1 - \gamma_1)\mathbf{f}_2(\mathbf{x})$, and any motion along that boundary is then well determined, as γ_1 must take a particular value that keeps $\mathbf{x}(t)$ in a neighbourhood of the boundary between $\mathcal{Q}_1$ and $\mathcal{Q}_2$. If $\mathbf{x}$ lies on the boundary between several modes then the space of $\{\gamma_1, \ldots, \gamma_m\}$ is larger than the tangent space of the boundary, so the γ_i are under-determined and become sensitive to other particulars of the simulation, such as the implementation of switching $\mathrm{Imp}(\mathbf{x}, M)$.

To find the effective motion eq. (5) along a discontinuity surface, we need to numerically find the constants γ_i for any given simulation, which we obtain using (4) as follows.

Let us take the simplest case of two hypersurfaces cutting space into four regions $\mathcal{Q}_1$,$\mathcal{Q}_2$,$\mathcal{Q}_3$,$\mathcal{Q}_4$. Without loss of generality we can take the hypersurfaces to be the coordinate hyperplanes $x = 0$ and $y = 0$ in coordinates $\mathbf{x} = (x, y, z)$ (as in fig. 1), as three dimensions will suffice to observe

motion along the intersection $x = y = 0$, and so let

$$\begin{aligned} \mathcal{Q}_1 &= \{(x,y,z):\ x>0, y>0\}\ , \qquad \mathcal{Q}_2 = \{(x,y,z):\ x<0, y>0\}\ , \\ \mathcal{Q}_3 &= \{(x,y,z):\ x<0, y<0\}\ , \qquad \mathcal{Q}_4 = \{(x,y,z):\ x>0, y<0\}\ . \end{aligned} \tag{6}$$

Assuming motion along an ε-neighbourhood of the intersection $x = y = 0$, define scaled coordinates $u = x/\varepsilon$, $v = y/\varepsilon$, and time $\tau = t/\varepsilon$. Denoting the time derivative with respect to τ by a prime, and the vector field components as $\mathbf{f} = (f, g, h)$, then if motion is given by (5) we have

$$u' = f_{\text{eff}}(\varepsilon u, \varepsilon v, z)\ , \quad v' = g_{\text{eff}}(\varepsilon u, \varepsilon v, z)\ , \quad z' = \mathcal{O}(\varepsilon)\ . \tag{7}$$

Since z is then slow-varying and $(u, v) = \mathcal{O}(\varepsilon)$ for small ε, we shall simulate (7) from an initial point $(u, v) = (0, 0)$, for different values of z treated as a static parameter. We then evolve the system for a long time $\Delta\tau$ and calculate the coefficients γ_i from (3). The time $\Delta\tau$ should be sufficiently long that $\Delta(u, v)/\Delta\tau$ reaches a steady value, hence the γ_i reach steady values, corresponding to the dynamics in x and y having settled upon an attractor in the neighbourhood of $x = y = 0$. (Provided the vector fields $\mathbf{f}_i$ point outward from every region $\mathcal{Q}_i$, solutions are confined to a neighbourhood of the boundary and such an attractor is guaranteed to exist, but may not be unique).

With the coefficients γ_i having been calculated, the expression (5) then gives the effective speed of sliding along $x = y = 0$ on the original timescale t. The third component defines the *speed of sliding*,

$$\dot{z} = h_{\text{slide}}(\mathbf{x}) = \gamma_1 h_1(\mathbf{x}) + \gamma_2 h_2(\mathbf{x}) + \gamma_3 h_3(\mathbf{x}) + \gamma_4 h_4(\mathbf{x}) \tag{8}$$

along the intersection, with $\gamma_1 + \gamma_2 + \gamma_3 + \gamma_4 = 1$.

A. Numerical example

We now set up an example on which to perform simulations. To observe jitter we need assume only that the vector fields $\mathbf{f}_i$ push solutions of (2) onto some portion of the discontinuity surfaces and their intersections.

Let us take the simplest case for the directions of the vector fields $\mathbf{f}_i$, namely that they point outwards from all of the regions $\mathcal{Q}_i$ (and therefore in towards the intersection). Expanding the vector fields $\mathbf{f}_i$ about the intersection $x = y = 0$,

$$\mathbf{f}_i(\mathbf{x}) = \hat{\mathbf{f}}_i(z) + \mathcal{O}(x, y) \tag{9}$$

and writing $\hat{\mathbf{f}}_i = (\hat{f}_i, \hat{g}_i, \hat{h}_i)$, this implies that the components of $\hat{\mathbf{f}}_i$ satisfy

$$\hat{f}_1, \hat{f}_4 < 0 < \hat{f}_2, \hat{f}_3 \qquad \& \qquad \hat{g}_1, \hat{g}_2 < 0 < \hat{g}_3, \hat{g}_4 \; . \tag{10}$$

For all of the implementations considered below, these conditions guarantee that solutions are trapped in a neighbourhood of $x = y = 0$, since each $\mathbf{f}_i$ produces decreasing values of $|x|$ and $|y|$.

For genericity we also assume that the four vector fields $\hat{\mathbf{f}}_i = (\hat{f}_i, \hat{g}_i, \hat{h}_i)$, are linearly independent. As we discuss in section 3, any piecewise-smooth vector field so defined will typically exhibit jitter, depending on how the equations are solved (or simulated) at the discontinuity.

Thus overall we simulate

$$\dot{\mathbf{x}} = \mathbf{f}(\mathbf{x}) = \begin{cases} \mathbf{f}_1(\mathbf{x}) \;\text{ for }\; x > 0,\; y > 0, \\ \mathbf{f}_2(\mathbf{x}) \;\text{ for }\; x < 0,\; y > 0, \\ \mathbf{f}_3(\mathbf{x}) \;\text{ for }\; x < 0,\; y < 0, \\ \mathbf{f}_4(\mathbf{x}) \;\text{ for }\; x > 0,\; y < 0, \end{cases} \tag{11}$$

where $\mathbf{f}_i = (f_i, g_i, h_i)$, and we neglect higher order terms from (9). As an example for demonstration we take

$$f_i(z) = a_i + A_i z, \quad g_i(z) = b_i + B_i z, \quad h_i(z) = c_i + C_i z, \tag{12}$$

where $a_i, b_i, c_i,$ and $A_i, B_i, C_i,$ are randomly generated constants taken in the range $(-1, +1)$, subject to the conditions (10) for $0 \le z \le 1$. We will use:

	a_i	A_i	b_i	B_i	c_i	C_i
$i = 1$	-0.5822	0.0384	-0.318	0.0994	-0.0410	-0.1498
$i = 2$	0.5408	0.1803	-0.1192	0.0135	0.2788	-0.382
$i = 3$	0.8700	-0.3475	0.9399	-0.8302	0.0896	-0.3578
$i = 4$	-0.2647	-0.7290	0.6456	-0.582	0.2948	0.2324

(13)

In section 2 B-2 F we simulate motion along $x = y = 0$ as described above, using different implementations $\mathrm{Imp}(\mathbf{x}, M)$ where the manner of switching across the surfaces $x = 0$ and $y = 0$ is perturbed by hysteresis, time delay, numerical discretization, smoothing, or noise. The key results, namely the speeds of sliding $\dot{z} = h_{\mathrm{slide}}$ for each implementation, are gathered together in fig. 3.

There are both disagreements and correlations between the different outcomes, which will require explanation. Here let us note only that all graphs lie within, and yet explore widely, the unshaded region of fig. 3. This unshaded region is the set of all possible speeds of sliding given by (8) as the γ_i take all allowed values, varying over in $0 \le \gamma_i \le 1$ subject to $\gamma_1 + \gamma_2 + \gamma_3 + \gamma_4 = 1$.

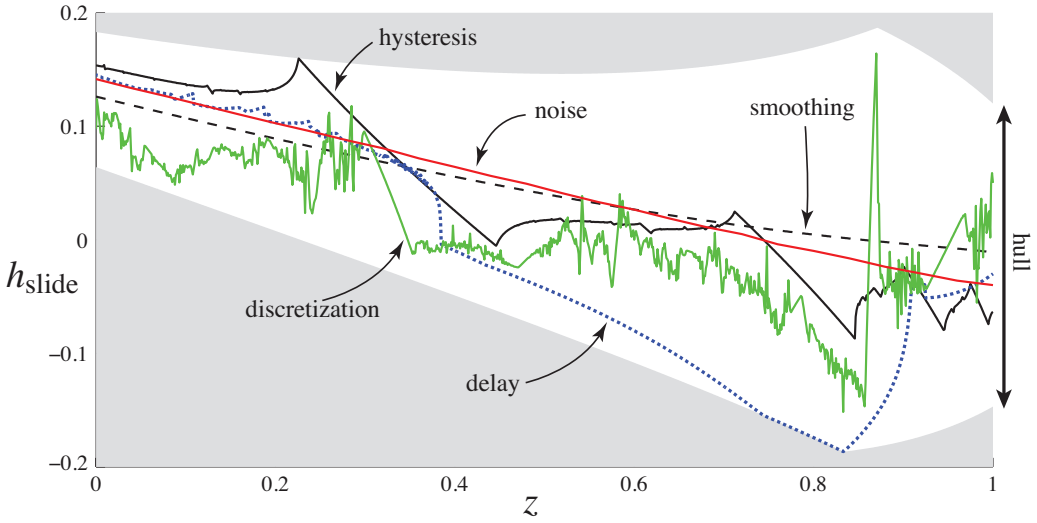

FIG. 3: The speed of sliding h_{slide} along $x = y = 0$ at different values of z for the piecewise-smooth system described above. The curves show the values of h_{slide} obtained if the switch is implemented as described in section 2 B-2 F: hysteresis (black), time-delay (blue dotted), discretization (green), smoothing (dashed), and white noise (red). The unshaded region is the convex hull formed by (8).

The results that follow are independent of the small parameter ε due to the simplicity of the example (11)-(12). In general this is not the case (as studied for example for the smoothing implementation in [16]).

B. Hysteresis

A common method for regularizing a switch between modes is hysteresis, used widely in electronics (see e.g. [1, 19–21]), and used as justification in [11] where the notion of sliding along a discontinuity was formally introduced.

Let switching occur with spatial delays α and β about $x = 0$ and $y = 0$ respectively. The implementation rule $\text{Imp}(\mathbf{x}, M)$ then corresponds to updating the mode $M \in \{1, 2, 3, 4\}$ when $x(t) = \pm\alpha$ or $y(t) = \pm\beta$, according to:

$$\begin{aligned}
&\bullet \quad \text{at } x = +\alpha,\ M \text{ updates as } \ 2 \mapsto 1 \text{ or } 3 \mapsto 4,\\
&\bullet \quad \text{at } x = -\alpha,\ M \text{ updates as } \ 1 \mapsto 2 \text{ or } 4 \mapsto 3,\\
&\bullet \quad \text{at } y = +\beta,\ M \text{ updates as } \ 3 \mapsto 2 \text{ or } 4 \mapsto 1,\\
&\bullet \quad \text{at } y = -\beta,\ M \text{ updates as } \ 2 \mapsto 3 \text{ or } 1 \mapsto 4.
\end{aligned} \tag{14}$$

The constants α and β are assumed to be small, and it will be convenient to define

$$\alpha = \varepsilon \cos(\phi\pi/2), \qquad \beta = \varepsilon \sin(\phi\pi/2), \tag{15}$$

for $0 < \varepsilon \ll 1$ and $0 < \phi < 1$. The ratio of α and β, now given by $\tan(\phi\pi/2)$, will prove to be important in simulations.

Note that if both $|x(t)| = \alpha$ and $|y(t)| = \beta$ at some time t, then two updates from (15) happen simultaneously, but this causes no ambiguity. For instance if an orbit in mode 1 reaches $(x(t), y(t)) = (-\alpha, -\beta)$ then the orbit changes to mode 3 (either via $i : 1 \mapsto 2 \mapsto 3$ or $i : 1 \mapsto 4 \mapsto 3$).

Using this implementation we then simulate the system (11)-(13), calculating the coefficients γ_i in (4), which provides the effective speed h_{slide} along the intersection as given by (8). As described in section 2 we simulate from an initial condition near $x = y = 0$ treating z as a parameter, running each simulation sufficiently long that each γ_i reaches a steady value, which corresponds to the dynamics in x and y reaching an attractor.

As we simulate the system, we obtain a trajectory in (x, y) space that bounces around inside the box $[-\alpha, +\alpha] \times [-\beta, +\beta]$, following straight line segments along the directions of the vector fields $\mathbf{f}_i$. These settle to a unique attractor after a sufficient time, two examples of which are shown in fig. 4 at different values of z (more precisely showing part of a numerically computed forward orbit with transient dynamics removed). In panel A the attractor has six switches per period. In panel B the attractor is either quasi-periodic or has such a high period that we were unable to detect it.

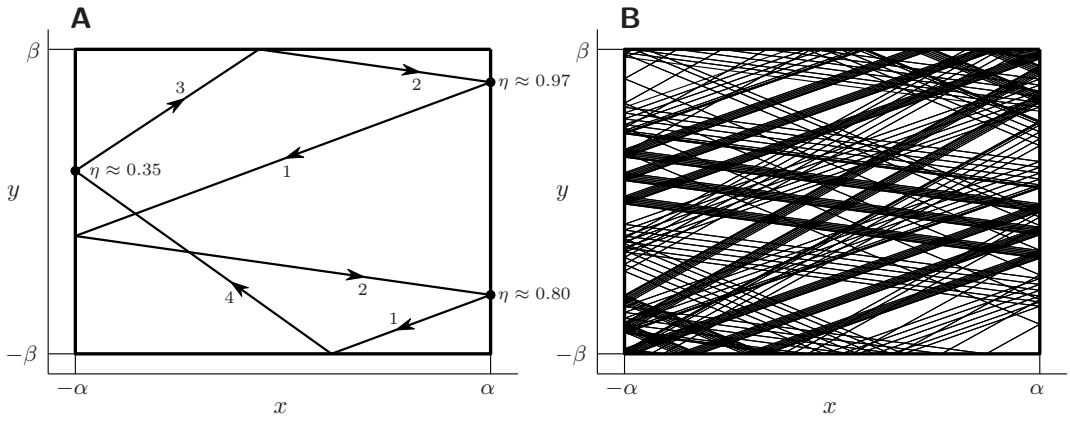

FIG. 4: Attractors in the chatterbox Ω (29) of the system (11)-(13) implemented with hysteresis. In panel A, $z = 0.3$; in panel B, $z = 0.5$. Both panels use $\phi = 0.5$, and the value of ε is arbitrary. In panel A the mode along different sections of the orbit is indicated, and at alternate vertices we give the value of η for the circle map defined later in section 4 B.

As discussed in section 2 A, the value of each γ_i in the speed of sliding (8) is defined as the

fraction of time that an orbit following the attractor spends in mode i. For the attractor shown in fig. 4-A, for example, we have $\gamma_1 = 0.35$, $\gamma_2 = 0.38$, $\gamma_3 = 0.08$ and $\gamma_4 = 0.19$, giving $h_{\text{slide}} = 0.10$ (to two decimal places).

By carrying out such a simulation at different values of z we obtain a graph of h_{slide}, shown in fig. 3. The attractor corresponding to the point $z = 0.3$ on the hysteresis graph in fig. 3, for example, is the orbit shown in fig. 4-A.

We can also fix z and calculate h_{slide} as the ratio $\alpha/\beta = \tan(\phi\pi/2)$ varies. This is plotted for two different z values in fig. 5.

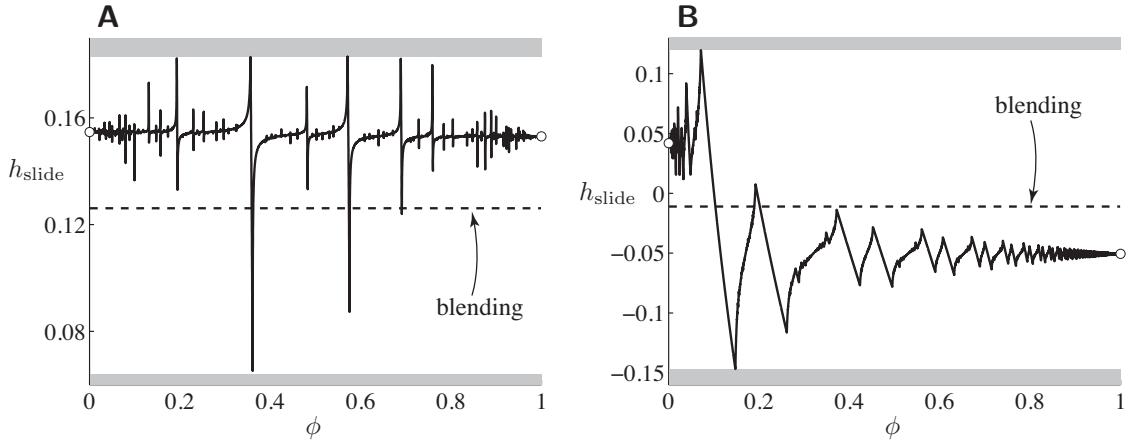

FIG. 5: The sliding vector field h_{slide} as a function of ϕ for the system (11)-(13) implemented with hysteresis, with $z = 0$ in panel A and $z = 1$ in panel B. The values of the graph at $\phi = 0$ and $\phi = 1$ are highlighted by circles, to be calculated later in proposition 4.3. The shaded upper and lower borders indicate the hull of all possible motions (see end of section 2 A). The dashed line indicates the result predicted by blending, which will be described in section 3.

The key features to note are the abrupt changes in the gradient of the graphs in both fig. 3 and fig. 5. Each smooth portion of the graph corresponds to a different attractor, two of which are illustrated in fig. 4. At the kinks of these graphs, one attractor is destroyed and another is born, causing a change in the time proportions γ_i spent in each mode, resulting in the corresponding sudden change in the sliding speed h_{slide}. We look more into these bifurcations in section 4.

C. Time-delay

An important feature of many mechanical control systems is time delay, where a control action taken in a system is based on information not of the current state $\mathbf{x}(t)$, but of the state some time

ε in the past, $\mathbf{x}(t-\varepsilon)$.

Here we consider the implementation $\mathrm{Imp}(\mathbf{x}, M)$ of switching to occur when $x(t-\varepsilon)$ or $y(t-\varepsilon)$ pass through the discontinuity surfaces $x = 0$ or $y = 0$, where some small $\varepsilon > 0$ represents a constant time-delay. This scenario was also considered briefly in [22]. More generally one could consider different delays across each discontinuity surface, but a single delay is sufficient here.

Simulating the system (11)-(13), and calculating the coefficients γ_i in (4) then provides the effective speed h_{slide} along the intersection $x = y = 0$ as given by (8), treating z as a parameter. As before we run each simulation sufficiently long that the γ_i reach steady values, when the dynamics in x and y reach an attractor.

The attractors at two different values of z are shown in fig. 6. If the trajectory crosses a surface $x = 0$ and $y = 0$ only once during the delay time ε then mode switching occurs along the dashed lines, otherwise the locus of switches is more complicated.

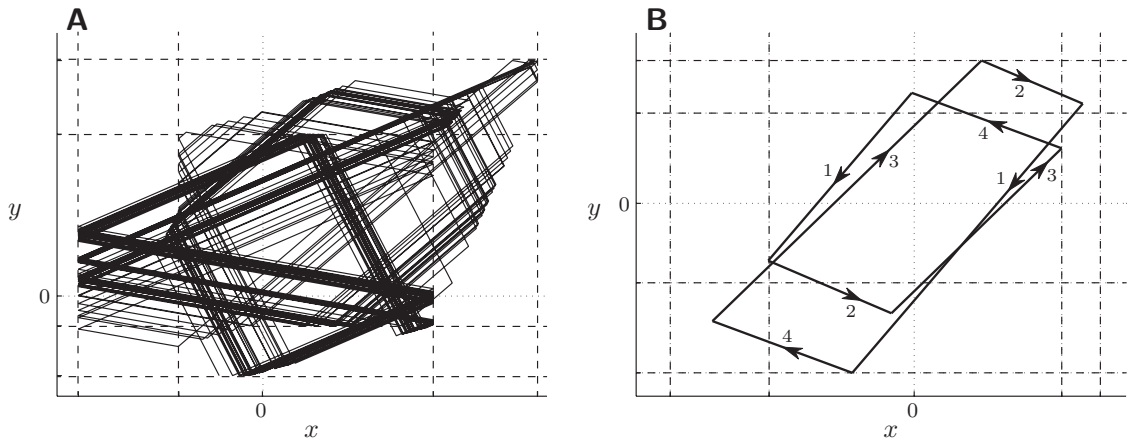

FIG. 6: Attractors of the system (11)-(13) implemented with time-delay, with $z = 0$ in panel A and $z = 0.9$ in panel B. The value of ε is arbitrary. In panel B there are two attracting periodic orbits. The modes along different portions of the orbit in B are indicated.

As with hysteresis, we observed that typically the attractor is periodic. By varying z and finding h_{slide} we produce the 'delay' graph in fig. 3.

A particular behaviour occurs for $0.74 \lesssim z \lesssim 0.83$, where we find $\gamma_4 = 0$, hence the attractor involves only the modes $i = 1, 2, 3$, and lies on the boundary of the unshaded region in fig. 3 whose significance we will describe in section 3.

Unlike with hysteresis, the time-delayed system can have multiple attractors (which remain distinct for $\varepsilon \to 0$), each corresponding to a distinct sliding speed of sliding along $x \approx y \approx 0$. With $z = 0.9$, for example, two distinct attractors have been identified as seen in fig. 6-B.

The presence of multiple attractors could allow for interesting (e.g. periodic) sliding dynamics in the full system (i.e. including variation in z), if motion is able to transfer between those attractors as z varies. This could lead, for example, not just to jittery motion along the intersection, but jitter-induced periodicity or chaos in the sliding dynamics. The potentially complex study of such phenomena is left for future work.

D. Discretization

Arguably the most important factor to understand in simulating dynamics with discontinuities is the effect of numerical discretization. There are some hints such as [23] of non-trivial dynamics resulting from discretizing a solution around a discontinuity surface when bifurcations are involved, but their effects remain as small perturbations of the ideal analytic (non-discretized) dynamics. We shall see here that jitter has much stronger implications.

Let us consider solving the system (11)-(13) using forward Euler iteration with step-size ε, that is, iterating the discrete system

$$\mathbf{x}_{i+1} = \mathbf{x}_i + \varepsilon \mathbf{f}(\mathbf{x}_i) \; . \tag{16}$$

About a single attracting discontinuity surface ($x = 0$ or $y = 0$), this generates a solution that rapidly switches or 'chatters' back-and-forth across the surface. (Moreover as $\varepsilon \to 0$ this solution converges to Filippov's solution, see for instance [24], which we describe in section 3).

The implementation $\mathrm{Imp}(\mathbf{x}, M)$ of switching now becomes to switch mode $M : i \mapsto i'$ whenever a sign change is detected between two steps x_i to x_{i+1}, or y_i to y_{i+1}, in coordinates $\mathbf{x}_i = (x_i, y_i, z_i)$. The switch therefore suffers a spatio-temporal delay similar to those in section 2 B-2 C, but dependent on the distance of the point $\mathbf{x}_i$ from the ideal discontinuity surface.

As before we run a simulation treating z as a parameter, over sufficiently many iterations that the γ_i reach steady values, when the dynamics in x and y reach an attractor. Calculating the coefficients γ_i in (4) then provides the effective speed h_{slide} along the intersection $x = y = 0$ as given by (8).

The discretization (16) is a two-dimensional piecewise-smooth map, made up of four continuous translations with discontinuities between them. The forward orbits are typically aperiodic and evenly fill a dense subset of some patterned region, let us call it Ψ. Figure 7 shows Ψ from simulations at two different values of z.

Our numerical investigations reveal that Ψ is often, but not always, unique. In this case Ψ

appears to be the closure of the ω-limit set of every initial point in the (x, y)-plane. The γ_i are then given by the fraction of Ψ contained in each quadrant of the (x, y)-plane. The region Ψ changes smoothly with z, except where it undergoes fundamental changes due to interactions with $x = 0$ and $y = 0$.

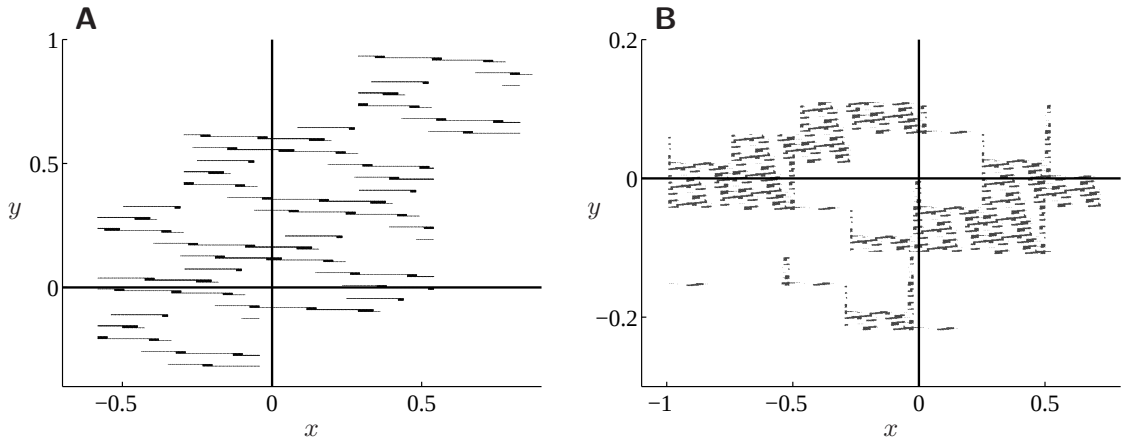

FIG. 7: Attractors Ψ of the system (11)-(13) discretized using (16). The value of ε is arbitrary. Shown at $z = 0$ in panel A, and $z = 1$ in panel B.

Figure 3 shows the resulting graph (labelled 'discretization') for h_{slide} as z varies. The sliding speeds generated are the most erratic of all the implementations, and therefore the greatest source of jittery dynamics.

A further study of the properties of the discrete map, the attractor Ψ, and the highly erratic jitter it generates, remains a challenge for future work.

E. Smoothing

Perhaps the simplest way to implement a discontinuity is to smooth it. The most common method is to smooth across the discontinuity surfaces $x = 0$ and $y = 0$ independently.

We first define a smooth *transition* function $\phi(u)$ that satisfies

$$\phi(u) \in \begin{cases} 1 & \text{for } u \geq +1 \,, \\ 0 & \text{for } u \leq -1 \,, \\ (0,1) & \text{for } |u| \leq 1 \,, \end{cases} \tag{17}$$

such that $\phi'(u) > 0$ for $|u| < 1$. The smoothing of (11) is then given by a bilinear interpolation

between the four vector fields $\mathbf{f}_i$,

$$\dot{\mathbf{x}} = \mathbf{f}_{sm}(\mathbf{x}) = [u_1\mathbf{f}_1(\mathbf{x}) + (1-u_1)\mathbf{f}_2(\mathbf{x})]u_2 + [(1-u_1)\mathbf{f}_3(\mathbf{x}) + u_1\mathbf{f}_4(\mathbf{x})](1-u_2) \tag{18}$$

where $u_1 = \phi(x/\varepsilon_1)$ and $u_2 = \phi(y/\varepsilon_2)$.

Such smoothings are a particular topic of interest as so-called *Sotomayor-Teixeira regularizations*, see e.g. [10, 15–17].

The implementation $\mathrm{Imp}(\mathbf{x}, M)$ in this case is a smooth transition from one mode $M = i$ to another $M = i'$ modulated by the transition function. Applying this to solve the system (11)-(13), simulating for sufficient time that the γ_i reach steady values, the dynamics in x and y reach an attractor which in this case is a unique point.

The effective speed h_{slide} along the intersection $x = y = 0$ as given by (8) is shown in fig. 3. The result is independent of the values of ε_1 and ε_2. This graph, unlike any of the implementations so far, exhibits a steadily varying sliding speed h_{slide} showing no jitter. This result will be explained in section 3.

F. Noise

Any physical system in which a discontinuity occurs may suffer systemic or environmental sources of noise. To study the effect of such perturbations, the ordinary differential equation $\dot{\mathbf{x}} = \mathbf{f}(\mathbf{x})$ can be converted to a stochastic differential equation by adding white noise of order ε, or by perturbing the discontinuity surfaces $x = 0$ and $y = 0$ themselves to some $x = \varepsilon\xi_x(t)$ and $y = \varepsilon\xi_y(t)$ where $\xi_x(t)$ and $\xi_y(t)$ are stochastic process. We will describe results for the former of these, but both yield similar results.

The addition of noise to a sliding solution was studied for some simple examples exhibiting symmetry in [22], and the idea of using noise to resolve ambiguity in forward evolution has been used previously for non-Lipschitz points of continuous vector fields [25–27], as well as two-folds of discontinuous vector fields [28, 29]. As we shall see, the effect of noise is counterintuitively *more* regular than other implementations considered so far.

Let us consider perturbing (11) to form a stochastic differential equation

$$d\mathbf{x}(t) = \mathbf{f}(\mathbf{x}(t))\,dt + \varepsilon D\,d\mathbf{W}(t)\ , \tag{19}$$

where $\mathbf{W}(t)$ is a standard two-dimensional vector Brownian motion, and D is a non-singular matrix that allows for different noise magnitudes in different directions. The implementation $\mathrm{Imp}(\mathbf{x}, M)$

is then a switch in mode whenever crossing of the discontinuity surfaces $x = 0$ or $y = 0$ is detected, but the state $\mathbf{x}(t) = (x(t), y(t), z(t))$ is stochastic. Despite the discontinuities in $\mathbf{f}$, the system (11)-(13) with (19) has a unique stochastic solution [30, 31].

Simulating as usual (but using the Euler-Maruyama method to solve the stochastic equations), for sufficient time that the γ_i reach steady values, and varying z as a static parameter, we obtain the 'noise' graph of the sliding speed h_{slide} shown in fig. 3. This sliding solution appears to be a smooth function of z, thus, similar to the smoothed system, not displaying jitter.

To further understand the origin of this sliding solution, rather than simply plotting the distribution of x and y points around their attractor in the ε-neighbourhood of $x = y = 0$, we use a probability density function. Let $p_{\text{trans}}(\mathbf{x}, t; \mathbf{x}_0)$ denote the transitional probability density function for (11) with (19). That is, given $\mathbf{x}(0) = \mathbf{x}_0$, for any measurable subset $E \subset \mathbb{R}^2$ and any $t > 0$, the probability that $\mathbf{x}(t) \in E$ is $\int_E p_{\text{trans}}(\mathbf{x}, t; \mathbf{x}_0)\, d\mathbf{x}$. If each $\mathbf{f}_i$ is directed inwards, then p_{trans} converges to a steady-state density $p(\mathbf{x})$ as $t \to \infty$, see fig. 8.

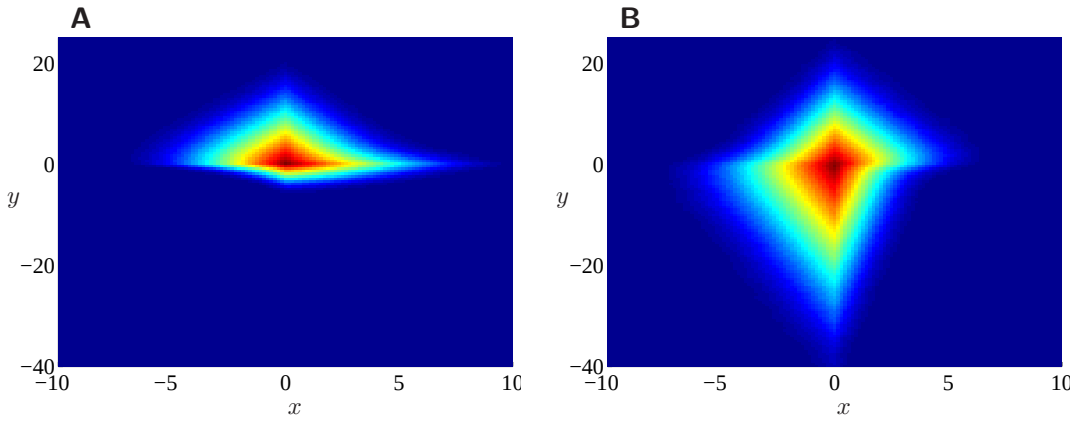

FIG. 8: Steady state probability density functions for the system (11)-(13) implemented with noise by (19) using $D = I$. The value of ε is arbitrary. In panel A, $z = 0$; in panel B, $z = 1$. The value of the probability density is indicated by shading (dark red = maximum value, dark blue = zero).

Since (11) with (19) is ergodic [32–34], the fraction of time γ_i spent in $\mathcal{Q}_i$ is equal to the spatial fraction of p over $\mathcal{Q}_i$. That is,

$$\gamma_i = \int_{\mathcal{Q}_i} p(\mathbf{x})\, d\mathbf{x}\,, \qquad i = 1, \ldots, 4\,. \tag{20}$$

Finally, we formulate a boundary value problem for p. It is a steady-state solution to the Fokker-Planck equation of (11) with (19), that is

$$-\nabla \cdot (\mathbf{f}p) + \frac{\varepsilon^2}{2} \nabla \cdot DD^{\mathsf{T}} \nabla p = 0\,, \qquad x \neq 0\,, y \neq 0\,. \tag{21}$$

Along $x = 0$ and $y = 0$ the density p is continuous and the 'flow of probability' across these boundaries is the same on each side. That is, the left and right limiting values of the probability current

$$J = \mathbf{n}^{\mathsf{T}}\left(\mathbf{f}p - \frac{\varepsilon^2}{2}DD^{\mathsf{T}}\nabla p\right), \tag{22}$$

are equal, where $\mathbf{n}$ is a unit normal vector to the boundary. This condition specifies the jump in the derivative of p at $x = 0$ and $y = 0$. Also $p \to 0$ as $|\mathbf{x}| \to \infty$.

Despite having a piecewise-constant drift vector $\mathbf{f}$ and a constant diffusion matrix D, we have been unable to obtain an analytical solution to this boundary value problem. This problem remains for future work.

3. NECESSARY CONDITIONS FOR JITTER

The previous section reveals that jitter occurs for some implementations of switching and not others. Moreover in fig. 3 it appears that jittery behaviour (from hysteresis, delay, discretization) may be contained within some definite range, while the jitter-free behaviour (from smoothing or noise) generate steady curves of a similar value. These basic observations, and certain necessary conditions for jitter, are easy to explain.

Returning to the general system (2), let us consider ideal switching across the discontinuity surfaces that bound the regions $\mathcal{Q}_i$. By ideal we mean that switching takes place at precisely the boundaries of the $\mathcal{Q}_i$, following infinitesimal increments of motion along each of the modes $\mathbf{f}_i$.

To define a solution of such an ideal system it is necessary to extend the dynamical equations (2) across the boundaries between the regions $\mathcal{Q}_i$. Following Filippov's theory of differential inclusions [11], this is achieved by taking the convex hull of $\mathbf{f}$ in an ε-neighbourhood of $\mathbf{x}$.

Definition 3.1. The *convex hull* of $\mathbf{f}(\mathbf{x})$ is the set

$$\mathbf{f}_{\text{conv}}(\mathbf{x}) = \bigcap_{\varepsilon>0} \text{Conv}\big(\mathbf{f}\big(\overline{\mathcal{B}}_\varepsilon(\mathbf{x})\big)\big), \tag{23}$$

where $\overline{\mathcal{B}}_\varepsilon(\mathbf{x})$ is the closed ball of radius ε centred at $\mathbf{x}$ and $\text{Conv}(\mathcal{F})$ denotes the convex hull of a set of vector fields $\mathcal{F}$.

A solution $\mathbf{x}(t)$ can then be defined as lying in the inclusion formed by the set-valued vector field (23).

Definition 3.2. A *Filippov solution* to $\dot{\mathbf{x}} = \mathbf{f}(\mathbf{x})$ is an absolutely continuous function $\mathbf{x}(t)$ for which $\dot{\mathbf{x}}(t) \in \mathbf{f}_{\text{conv}}(\mathbf{x}(t))$ for almost all t.

Applying this to the system (11)-(13) yields the set of allowed values of the sliding speed h_{slide} shown by the unshaded region in fig. 3. To show this, and to describe Filippov solutions in detail, a more explicit expression for the convex hull is required.

Since the hull is spanned by the vector fields $\mathbf{f}_i$, we can express $\mathbf{f}_{\text{conv}}$ as

$$\dot{\mathbf{x}} = \mathbf{f}_{\text{conv}}(\mathbf{x}) = \left\{ \sum_{i=1}^{m} \gamma_i \mathbf{f}_i(\mathbf{x}) \quad : \quad \gamma_i \geq 0, \quad \sum_{i=1}^{m} \gamma_i = 1 \right\}. \tag{24}$$

We recognise this as precisely the set of effective equations of motions (5). Hence the coefficients γ_i have the interpretation of being the proportions of time spent following each vector field $\mathbf{f}_i$ over an infinitesimal interval of time.

We have seen in section 2 that the coefficients can be calculated a posteriori once a solution has been simulated. We can alternatively ask whether the coefficients γ_i are determined a priori if we assume a certain qualitative form of motion. The simplest case is if we assume $\mathbf{x}(t) \in \mathcal{Q}_i$ for some interval of time, then $\gamma_i = 1$ and all other γ_j vanish for $j \neq i$, hence $\mathbf{f}_{\text{conv}}(\mathbf{x}) = \mathbf{f}_i(\mathbf{x})$.

The next simplest motion occurs if $\mathbf{x}$ lies on the boundary between just two modes, say $\mathcal{Q}_1$ and $\mathcal{Q}_2$, then (24) simplifies to $\mathbf{f}_{\text{conv}}(\mathbf{x}) = \gamma_1 \mathbf{f}_1(\mathbf{x}) + (1-\gamma_1)\mathbf{f}_2(\mathbf{x})$ (with $\gamma_3 = \gamma_4 = 0$ and $\gamma_2 = 1 - \gamma_1$). Assuming both vector fields point towards the boundary, the motion must proceed along it, implying $\mathbf{f}_{\text{conv}}(\mathbf{x})$ lies in the tangent space of the boundary. This provides one condition that is sufficient to find γ_1. For example if the boundary is $x = 0$, this implies the first component of $\mathbf{f}_{\text{conv}}(\mathbf{x})$ vanishes, which we write as $f_{\text{conv}}(\mathbf{x}) = \gamma_1 f_1(\mathbf{x}) + (1-\gamma_1) f_2(\mathbf{x}) = 0$, so that sliding motion along $x = 0$ is given by $\gamma_1 = f_2(\mathbf{x})/(f_2(\mathbf{x}) - f_1(\mathbf{x}))$. The motion then obtained along $x = 0$ is the standard concept of *sliding* along a discontinuity surface due to Filippov [11]. One can easily obtain similar expressions for motion along $x = 0 > y$, $x > 0 = y$, and $x < 0 = y$.

Since the γ_i are determined in these cases, sliding motion follows a steady, determinable function h_{slide}, given by (8) for the system (11). It is known that small perturbations of such sliding, via smoothing, spatio-temporal delays or noise, cause only small perturbations of h_{slide}, see e.g. [17, 28].

This fails when we consider motion along $x = y = 0$, where switching occurs between all four vector fields $\mathbf{f}_1$, $\mathbf{f}_2$, $\mathbf{f}_3$, $\mathbf{f}_4$. Motion along $x = y = 0$ implies $\dot{x} = 0$ and $\dot{y} = 0$. Applying these two conditions to (24) determines two of the coefficients γ_i (a third being determined since they sum to unity), leaving one of the γ_i undetermined. Hence the speed of sliding h_{slide} given by (8) along $x = y = 0$ takes a one-parameter family of possible values.

The set-valuedness of the convex hull (24) creates the freedom for solutions to explore a range of possible sliding motions, *if* switching is implemented in a manner that is well described by (5). This applies to implementations dominated by hysteresis, time delay, or discretization, as they

evolve in definite increments along each of the vector fields $\mathbf{f}_i$. The results of fig. 3 and fig. 5 appear to suggest that small perturbations of the implementation, such as changing the relative spatio-temporal delays associated with each discontinuity surface, producing graphs of h_{slide} that explore the convex hull in vastly different ways.

An alternative to the indeterminate result obtained from the convex hull (24), is to consider the convex *canopy* [10, 13]. This is a lower dimensional set of possible behaviours obtained by a bilinear interpolation or 'blending' across each discontinuity surface independently,

$$\dot{\mathbf{x}} = \mathbf{f}_{\text{can}}(\mathbf{x}) = \left\{ \begin{array}{l} \mu_y[\mu_x \mathbf{f}_1(\mathbf{x}) + (1-\mu_x)\mathbf{f}_4(\mathbf{x})] + \\ (1-\mu_y)[\mu_x \mathbf{f}_2(\mathbf{x}) + (1-\mu_x)\mathbf{f}_3(\mathbf{x})] \end{array} \quad : \quad \mu_y, \mu_x \in [0,1] \right\}. \tag{25}$$

The two conditions for sliding along $x = y = 0$, namely $f_{\text{can}} = g_{\text{can}} = 0$, are then sufficient to uniquely determine μ_x and μ_y, and uniquely predict the speed of sliding

$$\dot{z} = h_{\text{can}}(\mathbf{x}) = \left\{ \begin{array}{l} \mu_{y*}[\mu_{x*} h_1(\mathbf{x}) + (1-\mu_{x*})h_2(\mathbf{x})] + \\ (1-\mu_{y*})[\mu_{x*} h_3(\mathbf{x}) + (1-\mu_{x*})h_4(\mathbf{x})] \end{array} \quad : \quad \mu_{y*}, \mu_{x*} \in [0,1] \right\} \tag{26}$$

where μ_{y*} and μ_{x*} are solutions of the conditions $f_{\text{can}} = g_{\text{can}} = 0$.

When graphed on fig. 3 (or fig. 2), the canopy is found to coincide precisely with the sliding speed h_{slide} obtained from the smoothed simulation in fig. 3. In fact an equivalence is known to exist between the canopy and smoothings or 'regularizations', see e.g. [17, 18] and references therein. The correspondence to (18) is evident by replacing $\mu_x \mapsto u_1$ and $\mu_y \mapsto u_2$, hence when simulated, the smoothed system in section 2 E evolves to an attractor with steady values of x and y, resulting in steady values of u_1 and u_2, which correspond to steady values of the coefficients μ_x and μ_y. The reason for the noisy simulation in fig. 3 lying close to the same curve (a trend observed in numerous other simulations run by the authors), is less obvious.

More insight is provided by understanding the relation between (24) and (25). The coefficients μ_x and μ_y can be interpreted as proportions of time spent in $x > 0$ and $y > 0$ respectively. Hence by (6), μ_x is the proportion of time spent in mode $\mathcal{Q}_1$ or $\mathcal{Q}_4$, and μ_y is the proportion of time spent in mode $\mathcal{Q}_1$ or $\mathcal{Q}_2$, implying

$$\mu_x = \gamma_1 + \gamma_4 \,, \qquad \mu_y = \gamma_1 + \gamma_2 \,. \tag{27}$$

Substituting these into (24) we can then eliminate γ_2 and γ_4, and use the fact that the γ_i sum to unity to eliminate γ_3, then $\mathbf{f}_{\text{conv}}$ becomes (omitting the argument $\mathbf{x}$)

$$\begin{aligned} \mathbf{f}_{\text{conv}} &= \gamma_1 \mathbf{f}_1 + \gamma_2 \mathbf{f}_2 + \gamma_3 \mathbf{f}_3 + \gamma_4 \mathbf{f}_4 \\ &= \gamma_1 \mathbf{f}_1 + (\mu_y - \gamma_1)\mathbf{f}_2 + (1 - \mu_x - \mu_y + \gamma_1)\mathbf{f}_3 + (\mu_x - \gamma_1)\mathbf{f}_4 \,. \end{aligned} \tag{28}$$

Like (24) this still has three unknown coefficients μ_x, μ_y, and γ_1. However, if the proportions of time μ_x and μ_y are independent, then their product gives the proportion of time spent in mode $i = 1$ as $\gamma_1 = \mu_x\mu_y$. Substituting this into (28) yields (25), with only two unknown coefficients, μ_x and μ_y.

Hence the canopy (25) applies in cases where the rates of switching across the discontinuity surfaces $x = 0$ and $y = 0$ are independent, providing well defined coefficients μ_i and hence well defined motion for sliding along a discontinuity boundary. The hull (24) applies otherwise, in which case the coefficients γ_i are not uniquely determined and sliding motion is sensitive to perturbations, such as fine details of implementation.

Evidently from fig. 3, the smoothing of a bilinear interpolation between the vector fields $\mathbf{f}_i$, or stochastic switching between those vector fields, both behave as if the rates of switching across $x = 0$ and across $y = 0$ are independent. Such systems exhibit steady sliding motion which is well determined by the canopy (25).

For implementations that spend regular intervals of time in the different vector fields due to spatio-temporal delays (from hysteresis, time-delay, or discretization), fig. 3 instead suggests a dependence between the rates of switching across $x = 0$ and across $y = 0$, permitting solutions to explore more fully the hull (24). In doing so such implementations exhibit jitter, due to the sensitivity of the attractors that approximate to sliding along the neighbourhood of $x = y = 0$.

This is only a weak explanation of jitter, but provides necessary conditions for its occurrence. A rigorous explanation requires a detailed study of the attractors that constitute sliding motion along an intersection of discontinuity surfaces, such as the attractors in fig. 4 to 8. These require study of non-differentiable maps of dimension two (or more in general), or of a stochastic differential equation with discontinuities dimension two or more. Only in the case of hysteresis is this known to be reducible to a tractable problem.

4. THEORY OF HYSTERESIS-INDUCED JITTER

Here we summarize the theoretical results of Alexander and Seidman [9] for the hysteretic system (11) with (14). Their results are stated with equally sized hysteretic bands ($\phi = \frac{1}{2}$), but apply to any $\phi \in (0, 1)$ by a simple spatial scaling.

A. Chatterbox dynamics

If each $\mathbf{f}_i$ is directed inwards, as given by the conditions (12), then orbits of (11) with (14) cannot escape the rectangle

$$\Omega = \{(x, y) \ : \ |x| \leq \alpha, \, |y| \leq \beta\} \ . \tag{29}$$

Following [9], we refer to Ω as a *chatterbox*.

Recall that we write the vector fields in the regions $\mathcal{Q}_i$ as $\mathbf{f}_i = (f_i, g_i, h_i)$. Here it is convenient to let $\mathcal{F} = (f_1, \ldots, f_4)$ and $\mathcal{G} = (g_1, \ldots, g_4)$ be vectors containing the x and y-components of $\mathbf{f}$. Let $\Phi \subset \mathbb{R}^4 \times \mathbb{R}^4$ be the set of all $(\mathcal{F}, \mathcal{G})$ for which $(-f_i, -g_i) \in \mathcal{Q}_i$, for each i. Then each $(\mathcal{F}, \mathcal{G}) \in \Phi$ corresponds to a hysteretic system (11) with (14) for which each $\mathbf{f}_i$ is directed inwards.

Theorem 4.1. *Let $\varepsilon > 0$ and $\phi \in (0, 1)$. Then there exists an open dense subset $\tilde{\Phi} \subset \Phi$ such that, for all $(\mathcal{F}, \mathcal{G}) \in \tilde{\Phi}$, the hysteretic system* (11) *with* (14) *has an attracting periodic solution whose basin of attraction contains almost all points in Ω. Moreover, each γ_i is a Lipschitz function of $\mathcal{F}$ and $\mathcal{G}$, where γ_i denotes the fraction of time that the attracting periodic solution is in mode i.*

Alexander and Seidman prove theorem 4.1 by tiling the (x, y)-plane with copies of Ω so that (11) with (14) is reformulated as a doubly periodic vector field. From the theory of such vector fields [35], it immediately follows that the system has a unique rotation number for any $(\mathcal{F}, \mathcal{G}) \in \Phi$. For an open dense subset $\tilde{\Phi}$, this rotation number is rational and the system has an attracting periodic orbit. Most of the effort required to prove theorem 4.1 is in then using the piecewise-constant nature of the class of vector fields under consideration to show that there exists only one other invariant set: an unstable periodic orbit of the same period.

Theorem 4.1 tells us that the vector field h_{slide}, given by taking the $\varepsilon \to 0$ limit in the hysteretic system, is well-defined almost everywhere.

B. Circle map

The dynamics within Ω can be captured by a map on its boundary,

$$\delta\Omega = \{(x, y) \ : \ |x| = \alpha, \ |y| = \beta\} \ ,$$

between consecutive switching events. This map is discontinuous at the corners of Ω. It is better to work with the second return map on $\delta\Omega$ from the n^{th} switching event to the $(n+2)^{\text{th}}$ switching

event, which is continuous at the corners. With the labels defined as in eq. (6) and modes switching as in eq. (14), this map carries odd modes to odd, and even modes to even.

However, if we ignore switches at corners (which constitute a measure-zero subset), when an orbit switches its mode changes from even to odd or vice-versa. For this reason it is simpler to work with a map from the n^{th} switching point to the $(n+2)^{\text{th}}$ switching point.

Let (x, y) be any point on the boundary of Ω corresponding to an orbit $\mathbf{x}(t)$ that has just undergone a switch. By assuming that the mode of $\mathbf{x}(t)$ at this point is odd, the mode is completely determined by the point (x, y). Specifically, if (x, y) lies on either the top or right edge of Ω then $\mathbf{x}(t)$ is in mode 1 and if (x, y) lies on either the bottom or left edge of Ω then $\mathbf{x}(t)$ is in mode 3.

We map the boundary of Ω to a circle $\mathbb{S}^1$ by the continuous function

$$\eta = B(x,y) = \begin{cases} \frac{\alpha - x}{8\alpha} & \text{on } \ y = +\beta \ , \\ \frac{3\beta - y}{8\beta} & \text{on } \ x = -\alpha \ , \\ \frac{5\alpha + x}{8\alpha} & \text{on } \ y = -\beta \ , \\ \frac{7\beta + y}{8\beta} & \text{on } \ x = +\alpha \ . \end{cases} \tag{30}$$

The corners of Ω map under B to integer multiples of $\frac{1}{4}$.

Each $\eta \in \mathbb{S}^1$ corresponds to a point (x, y) on the boundary of Ω in either mode 1 or mode 3, as determined by the edge of Ω to which (x, y) belongs. For any $\eta \in \mathbb{S}^1$, we let $q(\eta) \in \mathbb{S}^1$ correspond to the location of the forward orbit of (x, y) immediately after its second switch.

Proposition 4.2. *Suppose each $\mathbf{f}_i$ is directed inwards. Then the circle map q is piecewise-linear, continuous, invertible, and degree-one.*

Proposition 4.2 is proved in Appendix A. Let $u_0 < \cdots < u_7$ be the ordered list of the values

$$\left\{0, \tfrac{1}{4}, \tfrac{1}{2}, \tfrac{3}{4}, q^{-1}(0), q^{-1}(\tfrac{1}{4}), q^{-1}(\tfrac{1}{2}), q^{-1}(\tfrac{3}{4})\right\} \ ,$$

and let $v_i = q(u_i)$ denote their images under q. The graph of q is then given by simply connecting each (u_i, v_i) to $\left(u_{(i+1) \bmod 8}, v_{(i+1) \bmod 8}\right)$ by a line segment (taking care to appropriately deal with the equivalence of $\eta = 0$ and $\eta = 1$). Figure 9 provides an example. Panel A shows the map q; panel B illustrates the action of q on each u_i (here the lines show the result of two excursions across the chatterbox and so do not align with the vector fields).

Figure 10 illustrates the circle map for the system (11)-(13), showing the attractors of fig. 4 in the context of the circle map. Figure 11 shows how the rotation number and period of the attractor in Ω varies over the entire range of ϕ and z values. There are open regions for which

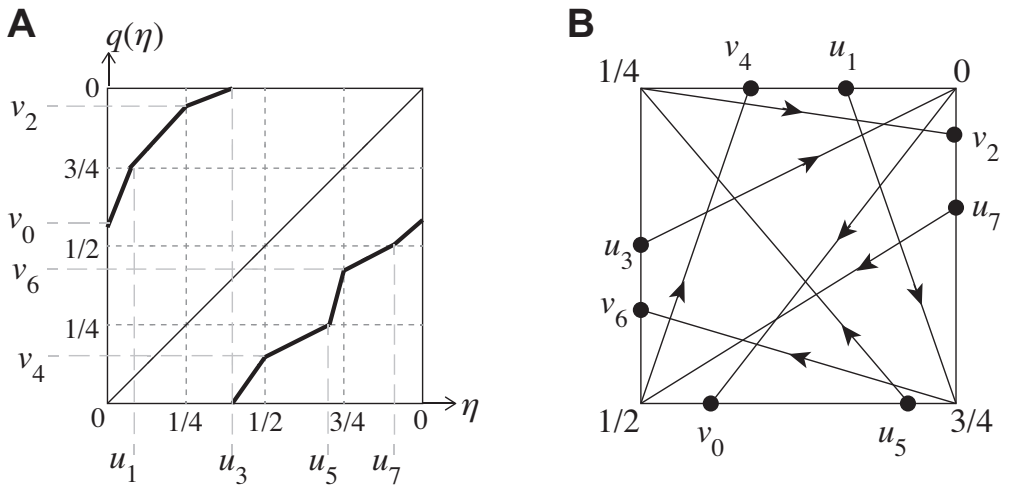

FIG. 9: Geometry of the second return map q. An example is shown in panel A: the points u_3, u_5, u_7, u_1, map to $\eta = 0, \frac{1}{4}, \frac{1}{2}, \frac{3}{4}$, which in turn map to v_0, v_2, v_4, v_6. This is illustrated in the chatterbox Ω in panel B.

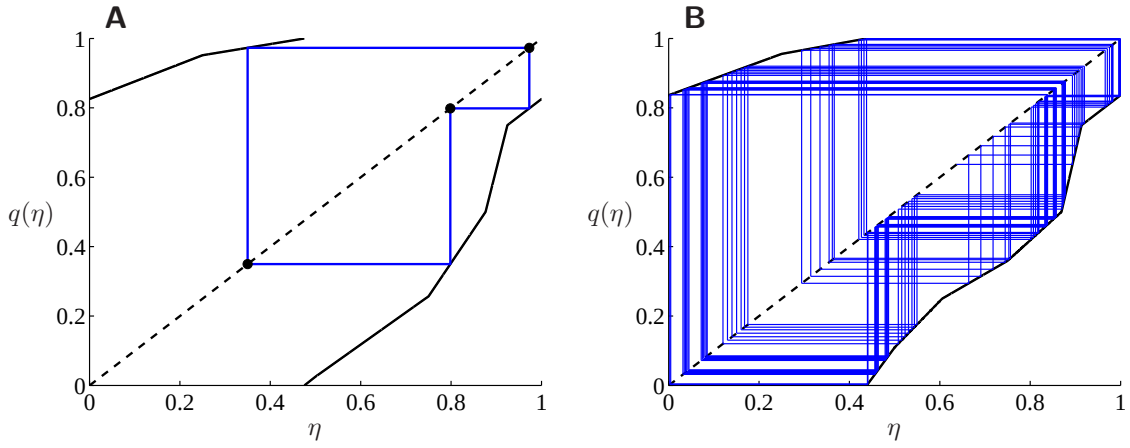

FIG. 10: Attractors of the circle map q for the system (11)-(13) with $\phi = 0.5$. In panel A, $z = 0.3$; in panel B, $z = 0.5$. These correspond to the attractors in Ω shown in fig. 4.

the rotation number is constant — these are *mode-locking regions*. By theorem 4.1 these regions densely fill parameter space. We observe that the mode-locking regions have points of zero width. This phenomenon has been described for the sawtooth map [36] and piecewise-linear maps on $\mathbb{R}^n$ [37, 38], but to our knowledge has not previously been detected for piecewise-linear maps whose slope takes more than two values.

The smooth portions of the hysteresis graph in fig. 3 correspond to attractors with a fixed rotation number. For instance between $z \approx 0.23$ to $z \approx 0.45$ the rotation number is $\frac{2}{3}$, as shown in fig. 11.

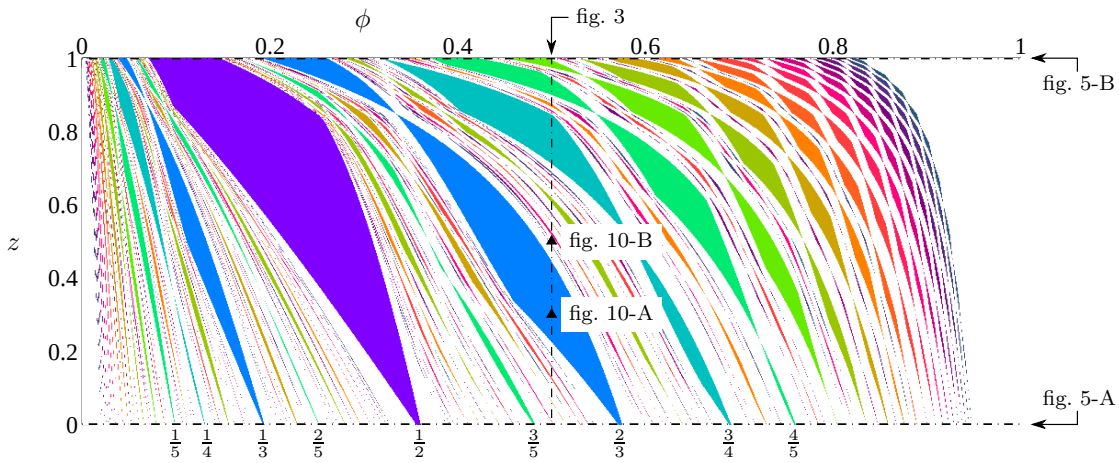

FIG. 11: Mode-locking regions of the circle map q for the system (11)-(13). Different colours correspond to different periods n up to $n = 20$; uncoloured regions correspond to a period $n > 20$ or a quasi-periodic orbit. At the bottom of the figure we have indicated the rotation numbers $\frac{m}{n}$ of mode-locking regions with $n \leq 5$. Figure 3, 10, and 5 correspond to cross-sections or particular points in this figure as indicated.

The two plots in fig. 5 correspond to horizontal cross-sections of fig. 11, and so we can see that while the rotation number is constant the value of h_{slide} varies smoothly. Over the range $\phi = 0$ to $\phi = 1$ the rotation number explores values across its full possible range (from 0 to 1). This forces intervals of constant rotation number to be relatively small and for this reason h_{slide} is an erratic function of ϕ.

C. The limiting hysteresis ratios

The value of h_{slide} can be given explicitly for the limits $\phi \to 0$ and $\phi \to 1$. With $\phi \approx 0$ or $\phi \approx 1$, the chatterbox Ω is a narrow rectangle. As orbits in Ω travel between the short sides of Ω they switch many times between two modes. During this time the motion is well-approximated by Filippov's standard sliding concept for a single discontinuity surface. We can then average the two sliding motions to obtain h_{slide}.

To state the limiting values of h_{slide} we require some additional notation. We let

$$\lambda_{14} = \frac{g_4}{g_4 - g_1}\,, \qquad \lambda_{23} = \frac{g_3}{g_3 - g_2}\,, \qquad \lambda_{12} = \frac{f_2}{f_2 - f_1}\,, \qquad \lambda_{43} = \frac{f_3}{f_3 - f_4}\,, \tag{31}$$

and for each of the four adjacent pairs of modes ij we let

$$\mathbf{f}_{ij} = \lambda_{ij}\mathbf{f}_i + (1 - \lambda_{ij})\mathbf{f}_j\,, \tag{32}$$

denote the sliding vector field. Writing $\mathbf{f}_{ij} = (f_{ij}, g_{ij}, h_{ij})$ we also let

$$\lambda_{14,23} = \frac{f_{23}}{f_{23} - f_{14}} , \qquad \lambda_{12,43} = \frac{g_{43}}{g_{43} - g_{12}} , \tag{33}$$

in order to average the corresponding pairs of $\mathbf{f}_{ij}$.

The following result, proved in App. B, provides the limiting values of γ_i from which h_{slide} is given by (8).

Proposition 4.3. *At any point on $x = y = 0$ at which each $\mathbf{f}_i$ of (11) is directed in towards $x = y = 0$, the zero-hysteresis sliding solution yields the following limiting values of γ_i. In the limit $\phi \to 0$,*

$$\gamma_1 = \lambda_{14,23}\lambda_{14} , \quad \gamma_2 = (1 - \lambda_{14,23})\lambda_{23} , \quad \gamma_3 = (1 - \lambda_{14,23})(1 - \lambda_{23}), \quad \gamma_4 = \lambda_{14,23}(1 - \lambda_{14}), \tag{34}$$

and in the limit $\phi \to 1$,

$$\gamma_1 = \lambda_{12,43}\lambda_{12} , \quad \gamma_2 = \lambda_{12,43}(1 - \lambda_{12}), \quad \gamma_3 = (1 - \lambda_{12,43})(1 - \lambda_{43}), \quad \gamma_4 = (1 - \lambda_{12,43})\lambda_{43} . \tag{35}$$

The values of h_{slide} obtained at these extrema are indicated by the white dots at $\phi = 0$ and $\phi = 1$ in fig. 5, confirming that the graph does indeed pass through these values.

D. Chatter box dynamics under weaker conditions

Jitter is possible under weaker conditions than discussed so far, where the intersection is not uniformly attracting. To demonstrate this let us illustrate hysteretic dynamics for piecewise-constant vector fields in three cases for which one or more of the $\mathbf{f}_i$ is not directed inwards, showing that jitter remains possible. The two cases are depicted by fig. 12.

Recalling that we write $\mathbf{f}_i = (f_i, g_i, h_i)$, we first consider

$$\begin{aligned} &f_1 = -1 , \quad g_2 = 1 , \qquad g_3 = 1 , \qquad g_4 = -1 , \\ &g_1 = 1.2 , \quad f_2 = -1.5 , \quad f_3 = 0.5 , \quad f_4 = 0.2 , \end{aligned} \tag{36}$$

see fig. 12-A. Here $\mathbf{f}_2$, $\mathbf{f}_3$ and $\mathbf{f}_4$ are directed inwards, but $\mathbf{f}_1$ is not. Nevertheless, the neighbourhood of the origin is a global attractor, because the sliding dynamics on $x = 0$ with $y > 0$ approaches $(x, y) = (0, 0)$.

When the system is perturbed by hysteresis, orbits repeatedly escape Ω (because $\mathbf{f}_1$ is not directed inwards) but remain within some neighbourhood of the origin (because the origin is an attractor of (11)). This is shown in fig. 13-A.

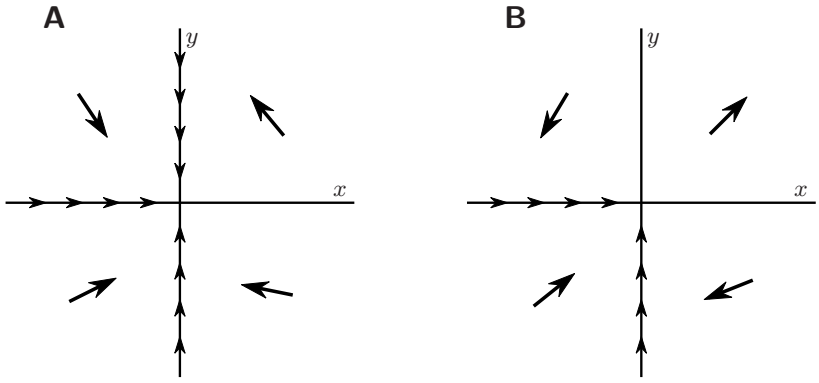

FIG. 12: Schematics of the two-dimensional piecewise-constant vector fields (11) considered below, with sliding motion on part of the discontinuity surfaces ($x = 0$ and $y = 0$).

Despite repeatedly escaping Ω, the map q from proposition 4.2 can be derived for this example and is shown in fig. 13-B. In this case q is discontinuous and is neither one-to-one nor onto, but the mere existence of the map and its possession of attractors mean that jitter is possible.

The third iterate of q is shown in fig. 13-B. For the given parameter values (36), and more generally for an open set of parameter values about them, there exists a trapping region within which the third iterate is given by a two-piece piecewise-linear function, as shown inset. This is a skew tent map with slopes 1 and $\frac{(g_1/f_1)(g_3/f_3)}{(g_2/f_2)(g_4/f_4)}$. With (36) the latter slope is -2. As described in [39–41], the dynamics is chaotic at these values. Similar to section 2, varying parameters or hysteresis ratios causes the attractor to undergo numerous bifurcations, and the dynamics along $x = y = 0$ therefore exhibits jitter. We leave further explorations of this to future work

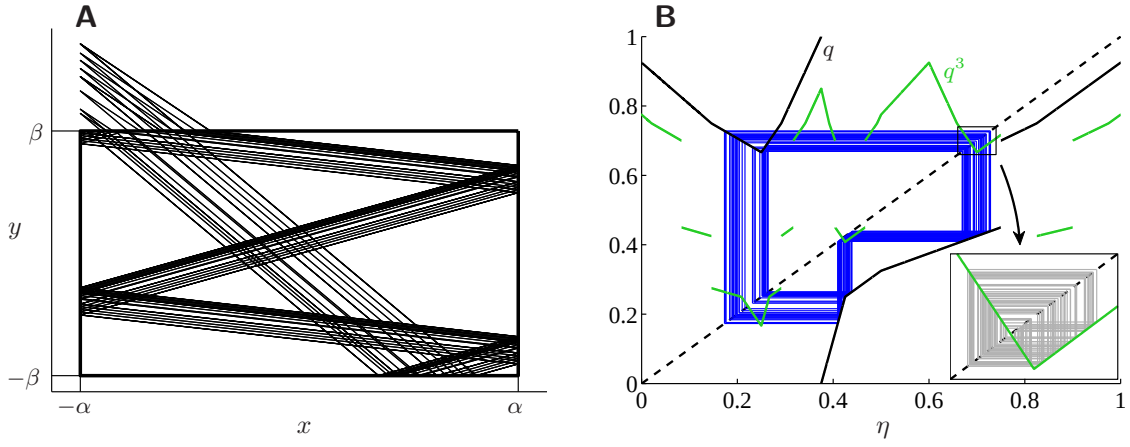

FIG. 13: The chaotic attractor of (11) with (14) and (36). Panel A shows part of an orbit in the (x, y)-plane; panel B shows the circle map q and its third iterate q^3.

Here we consider (11) with

$$\begin{aligned} f_1 &= 1\ , \quad f_2 = -0.6\ , \quad f_3 = 1\ , \qquad f_4 = -1\ , \\ g_1 &= 1\ , \quad g_2 = -1\ , \qquad g_3 = 0.8\ , \quad g_4 = -0.4\ , \end{aligned} \tag{37}$$

see fig. 12-B. This a representative example, the exact values as given are not important and are only provided for clarity. With these values $\mathbf{f}_1$ is directed outwards, hence the intersection $x = y = 0$ is not uniformly attracting, nevertheless orbits can become trapped in a neighbourhood of $x = y = 0$.

To understand why this occurs, first notice that the values (37) have been chosen such that for the unperturbed system (11), solutions on the negative x and y-axes approach the origin $(x, y) = (0, 0)$. Orbits thus approach the origin by either sliding along the negative x-axis, sliding along the negative y-axis, or regular motion in $x, y < 0$.

With the addition of hysteresis, such 'approaching' dynamics involves evolution with $x < \alpha$ and $y < \beta$ in modes 2, 3 and 4. But if an orbit is in mode 2, since $\mathbf{f}_2$ points towards $\mathcal{Q}_3$, the orbit cannot switch to mode 1 by reaching $x = \alpha$, it can only switch to mode 3 by reaching $y = -\beta$. Similarly, $\mathbf{f}_4$ points towards $\mathcal{Q}_3$ and so an orbit in mode 4 can only switch to mode 3. If an orbit in mode 3 reaches $y = \beta$ (with $x < \alpha$) it changes to mode 2, whilst if it reaches $y = \alpha$ (with $y < \beta$) it changes to mode 4. In the special case that it reaches $(x, y) = (\alpha, \beta)$ it changes to mode 1 (and subsequently escapes). Thus escape from a proximity to the origin requires passing through the point (α, β). Hence, over any finite time interval, almost all orbits remain near the origin. In this sense hysteresis stabilizes the unstable sliding surface $x = y = 0$. As a result an attractor exists that gives rise to sliding, and again varying parameters or hysteresis ratios causes the attractor to undergo numerous bifurcations, inducing jitter. We also leave further explorations of this to future work.

5. AN APPLIED EXAMPLE - ELECTRONIC POWER CONTROL

Power electronics seeks to regulate energy conversion in order to interface machinery with electrical power transfer systems. Often this is achieved using physical switches in the form of solid state semiconductor devices, for which a discontinuous on-off function is an accurate representation, see e.g. [20, 21], and has become an important part of their mathematical design, referred to as *variable structure*, *sliding mode*, or *equivalent* control systems.

Let us take a relatively simple example to illustrate jitter. We consider a circuit in which an inductor, two capacitors, and electrical switches are used to interface four electrical energy sources

in a theoretically lossless manner. This device is a basic example of a two-switch topology (e.g. [19]), and because of the independence of the switches, is found to exhibit jitter.

We assume that there are two voltage sources, E_1 and E_2, and two current sources, I_1 and I_2. There are four possible configurations of the system that are selected according to two independent switching conditions. The equations describing the system are

$$L\frac{di_L}{dt} = -(1-u_1)(1-u_2)v_{C_1} - (1-u_1)u_2E_1 + u_1(1-u_2)E_2 + u_1u_2v_{C_2} \tag{38}$$

$$C_1\frac{dv_{C_1}}{dt} = (1-u_1)(1-u_2)i_L - (1-u_2)I_1 + u_2I_2 \tag{39}$$

$$C_2\frac{dv_{C_2}}{dt} = -u_1u_2i_L + u_2I_1 - (1-u_2)I_2 \tag{40}$$

where u_1 and u_2 take the values 0 or 1. If these are chosen as

$$u_1 = H(i_L^* - i_L) \quad \text{and} \quad u_2 = H(v_{C_1}^* - v_{C_1}), \tag{41}$$

where H is the Heaviside step function, then the values of i_L and v_{C_1} are controllable provided $i_L, i_L^* < I_1$. An example of such a switched mode circuit with single-pole double-through switches is shown in Fig. 14.

Letting $x = (i_L - i_L^*)/A$, $y = (v_{C_1} - v_{C_1}^*)/V$, $z = v_{C_2}/V$, where A and V denote the units of current and voltage, and taking physically reasonable parameter values $L = 1.5mH$, $C_1 = 1.6mF$, $C_2 = 1.2mF$, $i_l^* = 3A$, $v_C^* = 10V$, $E_1 = 12V$, $E_2 = 10V$, $I_1 = 6A$, $I_2 = 4A$, the four modes become

$$(\dot{x}, \dot{y}, \dot{z}) = 10^3 \times \begin{cases} (-2(y+10)/3,\ 5(x-3)/8,\ -10/3)\ , & (x,y) \in \mathcal{Q}_1\ , \\ (20/3,\ -15/4,\ -10/3)\ , & (x,y) \in \mathcal{Q}_2\ , \\ (2z/3,\ 5/2,\ 5(3-x)/6)\ , & (x,y) \in \mathcal{Q}_3\ , \\ (-8,\ 5/2,\ 5)\ , & (x,y) \in \mathcal{Q}_4\ , \end{cases} \tag{42}$$

with the regions Q_i defined as in eq. (6).

We take hysteresis bounds $\alpha = \beta = \varepsilon/\sqrt{2}$ (so $\phi = 1/2$ in the notation of (15)). The simulations below are obtained approximating $x \approx y \approx 0$, which is valid for sufficiently small ε. In these simulations we use $\varepsilon = \sqrt{2}/10$ or $\varepsilon = \sqrt{2}/10^3$ (so that $\alpha = \beta = 0.1$ or 0.001).

Figure 15 shows two examples of the attractor between the hysteresis boundaries at fixed values of z. Figure 16 shows a simulation of the system obtained by solving the full system (38). The effect of jitter is observable as a marked change in the gradient, particularly around $t \approx 0.032s$. Two simulations for different hysteresis widths ε are shown, with similar results. The gradient, corresponding to the speed $\dot{z} = h_{\text{slide}}$, can be calculated numerically by taking the gradient of this

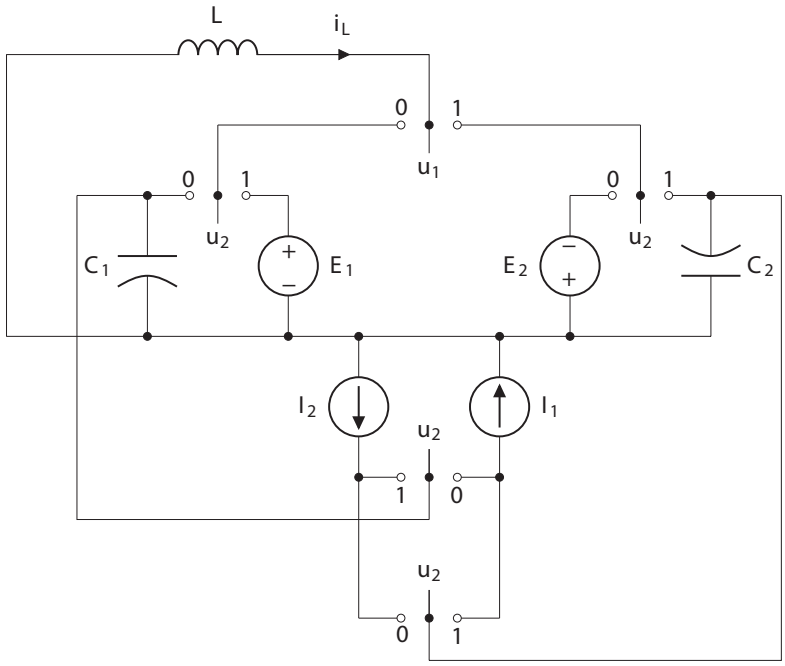

FIG. 14: Power transfer between sources using a switch network and passive elements. The variable controlling each switch (u_1, u_2) is shown above the switch itself; the position that the switch takes for input 1 is also marked. For input 0 the switch takes the complementary position.

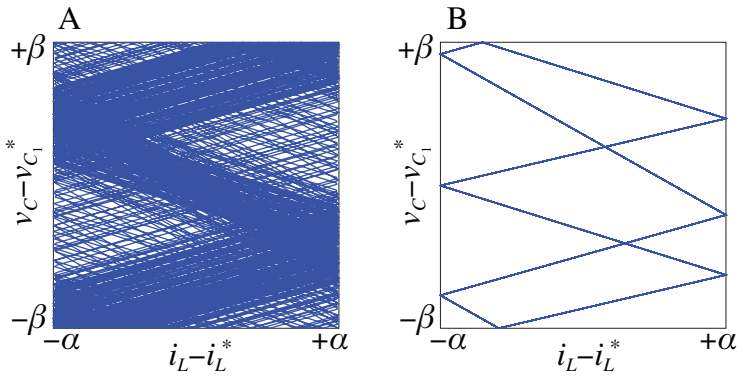

FIG. 15: Attractors inside the ε-hysteresis chatterbox at $z = v_{C_2} = 13$ (panel A) and $z = v_{C_2} = 16$ (panel B), with $\alpha = \beta = 0.1$.

graph, shown in panel B by the green dotted and red dashed curves for the two curves in panel A. This is compared in panel B to the theoretical sliding speed, found by iterating the hysteretic map inside the chatterbox at fixed z (thin blue curve), which corresponds to taking an ideal limit $\varepsilon = 0$, and which is almost indistinguishable from the $\varepsilon = \sqrt{2}/10^3$ simulation.

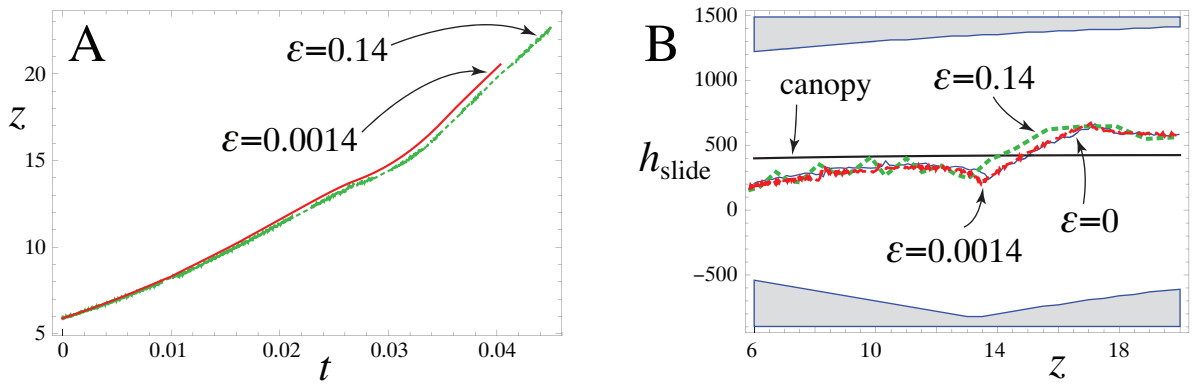

FIG. 16: Simulation of jitter in the circuit model for the parameters in fig. 15. Panel A shows a solution of the system (38) with $\varepsilon = \sqrt{2}/10^3$ (full curve) and $\varepsilon = \sqrt{2}/10$ (dotted curve). Panel B shows the speed along the switching intersection, calculated from the gradient of the full simulation for $\varepsilon = \sqrt{2}/10^3$ (dashed green curve) and $\varepsilon = \sqrt{2}/10$ (dotted red curve), and the ideal $\varepsilon = 0$ (thin blue curve) calculated by iterating the hysteretic map at fixed z. The $\varepsilon = \sqrt{2}/10^3$ and $\varepsilon = 0$ curves are almost indistinguishable. The canopy from (25) is also shown, and the unshaded region indicates the convex hull.

The results agree with the predicted theory, showing jitter in the sliding vector field, and in fig. 16-A we see how this affects the solution. In fig. 16-B we see that the derivative explores a significant portion of the convex hull, agreeing with the theoretical sliding motion given by the attractor in the chatterbox, and deviating significantly from the canopy combination. In the simulation with $\varepsilon = \sqrt{2}/10$, the switching frequency for u_1 is found to be more variable than the switching frequency of u_2, but for both it remains in a range between $5kHz$ and $25kHz$, which are within the operating range of widely used electronic sensors and semiconductor switches.

6. CLOSING REMARKS

The phenomenon of jitter along the intersection of multiple switches is a consequence of the rich dynamics that arises when switches are not ideal discontinuities, but instead involve elements of hysteresis, time-delay, or discretization. If we can assume that each coefficient $\mu_{x,y}$ in eq. (25) is determined independently, then their values are given by the canopy combination. This appears to be a good approximation for a system where the switch is a limit of a smooth sigmoid function which becomes infinitely steep, or of a noisy switch as the noise amplitude tends to zero. The canopy appears to be a poor approximation when hysteresis, time-delay, or discretization dominate the dynamics of switching, when instead the system evolves onto an attractor that determines

the dynamics, an attractor whose identity is sensitive to parameters of the vector fields and the switching model.

The attractor observed in the presence of hysteresis, time-delay, or discretization, is not obvious *a priori* from the vector fields, but is the solution of a continuous piecewise-differentiable circle map in the case of hysteresis, and more complicated maps in the cases of time-delay and discretization. The attractor undergoes bifurcations as parameters of the system are varied. These parameters may belong to the vector fields themselves, or to the perturbation. The bifurcations cause abrupt jumps in the attractor, resulting in abrupt jumps or 'jitter' in the dynamics along an intersection of switches. The work of Alexander and Seidman [9] showed that the sliding speed depends on the attractor at the intersection, and we have added to the explanation and details of the phenomenon, particularly its observable effect on the dynamics, showing that it extends to other perturbations. Clearly extensive further work is needed to study the attractors, and to derive rigorously the conditions for jitter, when delay, discretization, or noise are involved. The ultimate aim must be to understand systems that exhibit all of these non-idealities, and perhaps others (e.g. where the discontinuity surface itself is a fuzzy set or distribution), studying which perturbations dominate and what their influence is on the appearance of jitter. The effect would appear to be highly significant both for theoretical and practical problems involving interactions between two or more switches, so substantially deeper study is warranted.

Appendix A: Proof of proposition 4.2

Choose any $\eta \in \left(0, \frac{1}{4}\right)$ (other values can be treated similarly) and let $(x_0, y_0) = B^{-1}(\eta)$, where $y_0 = \beta$.

In mode i orbits follow $\dot{x} = a_i$ and $\dot{y} = b_i$. The forward orbit of (x_0, y_0) is initially in mode 1, where $a_1 < 0$ and $b_1 < 0$ because $\mathbf{f}_1$ is directed inwards. Thus the orbit next switches at either $x = -\alpha$ or $y = -\beta$. Let us suppose it switches at $x = -\alpha$ (the other case can be treated similarly). Let (x_1, y_1), where $x_1 = -\alpha$, denote the point of switching.

Now the orbit is in mode 2 for which $a_2 > 0$ and $b_2 < 0$. Thus it next switches at either $x = \alpha$ or $y = -\beta$. Let us suppose it switches at $x = \alpha$ (the other case can be treated similarly) and let (x_2, y_2), where $x_2 = \alpha$, denote the point of switching. Then $q(\eta) = B(x_2, y_2)$.

For sufficiently small $\Delta\eta > 0$ we have $\eta + \Delta\eta = B(x_0 - \Delta x, y_0)$, where $\Delta x = 8\alpha\Delta\eta$. For sufficiently small $\Delta\eta > 0$, the forward orbit of $(x_0 - \Delta x, y_0)$ next switches at $\left(x_1, y_1 + \frac{b_1 \Delta x}{a_1}\right)$ and

then at $\left(x_2, y_2 + \frac{b_1 \Delta x}{a_1}\right)$. Then

$$q(\eta + \Delta\eta) = B\left(x_2, y_2 + \frac{b_1 \Delta x}{a_1}\right) = \eta + \frac{b_1 \Delta x}{8\beta a_1} = \eta + \frac{\alpha b_1 \Delta \eta}{\beta a_1} \,,$$

and so $q'(\eta) = \frac{\alpha b_1}{\beta a_1} > 0$. Indeed in every case the value of $q'(\eta)$ is a positive constant. This demonstrates that q is piecewise-linear and, once we prove continuity at corners, is continuous and increasing.

Now suppose the forward orbit of (x_0, y_0) first switches at the corner $(-\alpha, -\beta)$. In this case $q(\eta) = \frac{1}{2}$ and the forward orbit of $(x_0 - \Delta x, y_0)$ switches at $\left(-\alpha, -\beta + \frac{b_1 \Delta x}{a_1}\right)$ and then at $\left(-\alpha - \frac{a_2 b_1 \Delta x}{b_2 a_1}, -\beta\right)$. Thus $q(\eta + \Delta\eta) = \frac{1}{2} + \mathcal{O}(\Delta\eta)$ which shows that q is continuous here. Similar arguments show that q is continuous at all corners and pre-images of corners of Ω.

Finally let us consider $q^{-1}(\eta)$ for any $\eta \in \left(0, \frac{1}{4}\right)$. The corresponding orbit that arrives at $(x_0, y_0) = B^{-1}(\eta)$ changes to mode 1, thus must previously have been in mode 4. The backward orbit of (x_0, y_0) is mode 4 is unique, and in this way we can follow the orbit backwards through two switches to verify that $q^{-1}(\eta)$ is well-defined and unique. That is, q is invertible, and since q is increasing it must be degree-one.

Appendix B: Proof of proposition 4.3

Here we prove the result for $\phi = 0$; the result for $\phi = 1$ follows by symmetry.

First consider an orbit as it travels from any point on the right boundary of Ω, $x = \alpha$, until reaching the left boundary, $x = -\alpha$. During this time the orbit switches between modes 1 and 4. With $\phi \approx 0$, the number of switches is $\mathcal{O}\left(\frac{1}{\phi}\right)$. Thus the fraction of time spent in mode 1 is $\tilde{\lambda}_{14} = \lambda_{14} + \mathcal{O}(\phi)$, and the fraction of time spent in mode 4 is $1 - \tilde{\lambda}_{14}$. Also the time taken to travel from $x = \alpha$ to $x = -\alpha$ is

$$T_{14} = \frac{-2\alpha}{\tilde{\lambda}_{14} f_1 + (1 - \tilde{\lambda}_{14}) f_4} \,. \tag{B1}$$

Upon reaching $x = -\alpha$, the orbit subsequently travels back to $x = \alpha$ switching between modes 2 and 3. The fraction of time spent in mode 2 is $\tilde{\lambda}_{23} = \lambda_{23} + \mathcal{O}(\phi)$, and the fraction of time spent in mode 3 is $1 - \tilde{\lambda}_{23}$. Also the time taken to travel from $x = -\alpha$ to $x = \alpha$ is

$$T_{23} = \frac{2\alpha}{\tilde{\lambda}_{23} f_2 + (1 - \tilde{\lambda}_{23}) f_3} \,. \tag{B2}$$

By combining these observations, we see that as the orbit travels from $x = \alpha$ until it next arrives at this boundary, the fraction of time spent in mode 1, for instance, is $\frac{T_{14}\tilde{\lambda}_{14}}{T_{14}+T_{23}}$. Since this is true

between any consecutive times at which the orbit is located on $x = \alpha$, it is also true for evolution over all $t \in \mathbb{R}$. Hence $\gamma_1 = \frac{T_{14}\tilde{\lambda}_{14}}{T_{14}+T_{23}}$. By using (B1) and (B2) it is readily seen that this value limits to the value of γ_1 in (34) as $\phi \to 0$. The values of γ_2, γ_3 and γ_4 in (34) follow in the same fashion from the above observations.

---

[1] V. Utkin, J. Guldner, and J. Shi. *Sliding Mode Control in Electro-Mechanical Systems.* CRC Press, Boca Raton, FL, 1999.

[2] J. Wojewoda, A. Stefański, M. Wiercigroch, and T. Kapitaniak. Hysteretic effects of dry friction: modelling and experimental studies. *Phil. Trans. R. Soc. A*, 366:747–765, 2008.

[3] H. Olsson, K.J. Åström, C. Canudas de Wit, M. Gäfvert, and P. Lischinsky. Friction models and friction compensation. *Eur. J. Control*, 4:176–195, 1998.

[4] M.R. Jeffrey, A.R. Champneys, M. di Bernardo, and S.W. Shaw. Catastrophic sliding bifurcations and onset of oscillations in a superconducting resonator. *Phys. Rev. E*, 81:016213, 2010.

[5] H. Kaper and H. Engler. *Mathematics and Climate.* SIAM, Philadelphia, 2013.

[6] Yu.A. Kuznetsov, S. Rinaldi, and A. Gragnani. One-parameter bifurcations in planar Filippov systems. *Int. J. Bifurcation Chaos*, 13(8):2157–2188, 2003.

[7] S.H. Piltz, M.A. Porter, and P.K. Maini. Prey switching with a linear preference trade-off. *SIAM J. Appl. Dyn. Sys.*, 13(2):658–682, 2014.

[8] A. Gabovich, editor. *Superconductors – Materials, Properties and Applications.* InTech, 2012.

[9] J.C. Alexander and T.I. Seidman. Sliding modes in intersecting switching surfaces, II: Hysteresis. *Houston, J. Math.*, 25:185–211, 1999.

[10] J.C. Alexander and T.I. Seidman. Sliding modes in intersecting switching surfaces, I: Blending. *Houston, J. Math.*, 24:545–569, 1998.

[11] A.F. Filippov. *Differential Equations with Discontinuous Righthand Sides.* Kluwer Academic Publishers., Norwell, 1988.

[12] L. Dieci and L. Lopez. Sliding motion on discontinuity surfaces of high co-dimension. A construction for selecting a Filippov vector field. *Numer. Math.*, 117:779–811, 2011.

[13] M.R. Jeffrey. Dynamics at a switching intersection: Hierarchy, isonomy, and multiple sliding. *SIAM J. Appl. Dyn. Syst.*, 13(3):1082–1105, 2014.

[14] L. Dieci and F. Difonzo. The moments sliding vector field on the intersection of two manifolds. To appear: *J. Dyn. Diff. Equat.*, 2015.

[15] J. Llibre, P.R. da Silva, and M.A. Teixeira. Sliding vector fields for non-smooth dynamical systems having intersecting switching manifolds. *Nonlinearity*, 28(2):493–507, 2015.

[16] N. Guglielmi and E. Hairer. Classification of hidden dynamics in discontinuous dynamical systems. *SIAM J. Appl. Dyn. Syst.*, 14(3):1454–1477, 2015.

[17] M.A. Teixeira and da Silva P.R. Regularization and singular perturbation techniques for non-smooth systems. *Phys. D*, 241:1948–1955, 2012.

[18] D. Panazzolo and P.R. da Silva. Regularization of discontinuous foliations: Blowing up and sliding conditions via Fenichel theory. *J. Diff. Eq.*, 263:8362–8390, 2017.

[19] H. Sira-Ramirez. Sliding motions in bilinear switched networks. *IEEE Trans. Circuits Systems*, CAS-34(8):919–933, 1987.

[20] V.I. Utkin. Sliding mode control design principles and applications to electric drives. *IEEE Trans. Ind. Electron.*, 40(1):23–36, 1993.

[21] S.-C. Tan, Y.M. Lai, and C.K. Tse. General design issues of sliding-mode controllers in DC-DC converters. *IEEE Trans. Ind. Electron.*, 55(3):1160–1174, 2008.

[22] E.A. Asarin and R.N. Izmailov. Determining the sliding speed on a discontinuity surface. *Automat. Remote Contr.*, 50(9):1181–1185, 1989. Translation of *Avtomatika i Telemekhanika*, 9:43-48, 1989.

[23] P. Glendinning and P. Kowalczyk. Micro-chaotic dynamics due to digital sampling in hybrid systems of Filippov type. *Phys. D*, 239:58–71, 2010.

[24] A. Dontchev and F. Lempio. Difference methods for differential inclusions: A survey. *SIAM Rev.*, 34(2):263–294, 1992.

[25] R. Bafico and P. Baldi. Small random perturbations of Peano phenomena. *Stochastics*, 6(3-4):279–292, 1982.

[26] F. Flandoli and J.A. Langa. Markov attractors: A probabilistic approach to multivalued flows. *Stoch. Dyn.*, 8(1):59–75, 2008.

[27] V.S. Borkar and K. Suresh Kumar. A new Markov selection procedure for degenerate diffusions. *J. Theor. Probab.*, 23:729–747, 2010.

[28] D.J.W. Simpson. On resolving singularities of piecewise-smooth discontinuous vector fields via small perturbations. *Discrete Contin. Dyn. Syst.*, 34(9):3803–3830, 2014.

[29] D.J.W. Simpson and M.R. Jeffrey. Fast phase randomisation via two-folds. *Proc. R. Soc. A*, 472(2186):20150782, 2016.

[30] D. Stroock and S.R.S Varadhan. Diffusion processes with continuous coefficients. I. *Comm. Pure Appl. Math.*, 22:345–400, 1969.

[31] N.V. Krylov and M. Röckner. Strong solutions of stochastic equations with singular time dependent drift. *Probab. Theory Relat. Fields*, 131:154–196, 2005.

[32] A.V. Skorokhod. *Asymptotic Methods in the Theory of Stochastic Differential Equations.* American Mathematical Society, Providence, 1989.

[33] R. Khasminskii. *Stochastic Stability of Differential Equations.* Springer, New York, 2010.

[34] V. Capasso and D. Bakstein. *An Introduction to Continuous-Time Stochastic Processes.* Birkhäuser, New York, 2015.

[35] V.I. Arnol'd. *Geometrical Methods in the Theory of Ordinary Differential Equations.* Springer-Verlag, New York, 1988.

[36] W.-M. Yang and B.-L. Hao. How the Arnol'd tongues become sausages in a piecewise linear circle map. *Comm. Theoret. Phys.*, 8:1–15, 1987.

[37] D.J.W. Simpson and J.D. Meiss. Shrinking point bifurcations of resonance tongues for piecewise-smooth, continuous maps. *Nonlinearity*, 22(5):1123–1144, 2009.

[38] D.J.W. Simpson. The structure of mode-locking regions of piecewise-linear continuous maps: I. Nearby mode-locking regions and shrinking points. *Nonlinearity*, 30(1):382–444, 2017.

[39] Yu.L. Maistrenko, V.L. Maistrenko, and L.O. Chua. Cycles of chaotic intervals in a time-delayed Chua's circuit. *Int. J. Bifurcation Chaos.*, 3(6):1557–1572, 1993.

[40] H.E. Nusse and J.A. Yorke. Border-collision bifurcations for piecewise-smooth one-dimensional maps. *Int. J. Bifurcation Chaos.*, 5(1):189–207, 1995.

[41] M. di Bernardo, C.J. Budd, A.R. Champneys, and P. Kowalczyk. *Piecewise-smooth Dynamical Systems. Theory and Applications.* Springer-Verlag, New York, 2008.

[42] M.R. Jeffrey. Exit from sliding in piecewise-smooth flows: deterministic vs. determinacy-breaking. *Chaos.*, Chaos 26 033108:1-20, 2016.

[43] R. Edwards and L. Glass. Dynamics in genetic networks. *Amer. Math. Monthly*, 121(9):793–809, 2014.